NASA TECHNICAL NOTE

NASA TN D-6894

NASA TN D-6894

DRAG CHARACTERISTICS OF A DISK-GAP-BAND PARACHUTE WITH A NOMINAL DIAMETER OF 1.65 METERS AT MACH NUMBERS FROM 2.0 TO 3.0

by Robert J. Mayhue and Percy J. Bobbitt

Langley Research Center
Hampton, Va. 23365

NATIONAL AERONAUTICS AND SPACE ADMINISTRATION • WASHINGTON, D. C. • OCTOBER 1972

1. Report No.	2. Government Accession No.	3. Recipient's Catalog No.
NASA TN D-6894		

4. Title and Subtitle	5. Report Date
DRAG CHARACTERISTICS OF A DISK-GAP-BAND PARACHUTE WITH A NOMINAL DIAMETER OF 1.65 METERS AT MACH NUMBERS FROM 2.0 TO 3.0	October 1972
	6. Performing Organization Code

7. Author(s)	8. Performing Organization Report No.
Robert J. Mayhue and Percy J. Bobbitt	L-8357
	10. Work Unit No.
9. Performing Organization Name and Address	117-07-04-01
NASA Langley Research Center Hampton, Va. 23365	11. Contract or Grant No.
	13. Type of Report and Period Covered
12. Sponsoring Agency Name and Address	Technical Note
National Aeronautics and Space Administration Washington, D.C. 20546	14. Sponsoring Agency Code

15. Supplementary Notes

16. Abstract

Supersonic wind-tunnel tests were conducted with disk-gap-band parachute models having a nominal diameter of 1.65 meters and geometric porosities of 10.0, 12.5, and 15.0 percent. Canopy inflation characteristics, angles of attack, and drag performance are presented for deployment behind forebody base extensions which were free to oscillate in pitch and yaw. The effect of increasing suspension-line length on canopy motions and drag performance is included, and the drag performance of a model with 12.5 percent geometric porosity is compared with results from flight tests of a parachute with a nominal diameter of 12.19 meters.

17. Key Words (Suggested by Author(s))	18. Distribution Statement
Supersonic drag of disk-gap-band parachute	Unclassified – Unlimited

19. Security Classif. (of this report)	20. Security Classif. (of this page)	21. No. of Pages	22. Price*
Unclassified	Unclassified	40	$3.00

*For sale by the National Technical Information Service, Springfield, Virginia 22151

DRAG CHARACTERISTICS OF A DISK-GAP-BAND PARACHUTE WITH A NOMINAL DIAMETER OF 1.65 METERS AT MACH NUMBERS FROM 2.0 TO 3.0

By Robert J. Mayhue and Percy J. Bobbitt
Langley Research Center

SUMMARY

A ground-test program has been conducted by the Langley Research Center to investigate supersonic drag characteristics of the disk-gap-band parachute being considered for a Mars landing mission. Scaled versions of a parachute that was flight-tested with a nominal diameter of 12.19 meters and a geometric porosity of 12.5 percent were deployed and inflated in the Propulsion Wind Tunnel facility at the Arnold Engineering Development Center, Tullahoma, Tennessee. The parachute models had a nominal diameter of 1.65 meters with geometric porosities of 10.0, 12.5, and 15.0 percent. The parachute models were attached to a forebody base extension which was free to pitch in any plane (no roll or translation). With the addition of a conical skirt, geometry of the base extension was changed from a cylindrical to a conical configuration. Trailing distances between the base extension and the leading edge of the inflated parachute were at about 13.4 base-extension diameters for the cylindrical configuration and about 6.7 diameters for the conical configuration. Ratios of canopy average nominal diameter to the maximum diameter of the base extensions were about 11.0 and 5.5 with the cylindrical and conical base extensions, respectively. One test was made to determine the effect of longer suspension lines on drag performance using the conical base extension. Trailing distance for this test was at about 9.6 base-extension diameters. Mach number range for all the tests was from 2.0 to 3.0 at a dynamic pressure of 3352 newtons per square meter.

Tensiometer and load-cell measurements, along with motion-picture films, provided data up to canopy angles of attack of about 20°. These data showed that the parachute models exhibited variations in canopy projected areas that were similar in amplitude to large-scale flight results but were increased in frequency by the inverse of the diameter ratios. These inflation characteristics resulted in low-frequency variations of average drag which were also similar in character to flight measurements. Canopy-inflation characteristics did not appear to be coupled with the angle-of-attack variations, but the fluctuations became more pronounced as the test Mach number was increased from 2.0 to 3.0. Variations in geometric porosities of 10.0, 12.5, and 15.0 percent had little effect on canopy-inflation areas and drag. Change from a cylindrical to a conical base extension,

with a corresponding change in trailing distance from 13.4 to 6.7 base-extension diameters, resulted in a reduction in parachute drag of about 5 percent over the test Mach number range. Fluctuations in canopy inflation and angles of attack were alleviated with the conical base extension. Increasing the length of the suspension lines from 6.7 to 9.6 diameters behind the conical base extension produced an increase in drag of about 30 percent at a Mach number of 2.5. This improvement, however, was accompanied by pronounced fluctuations in canopy profile shape and a significant increase in canopy angles of attack.

Comparison of the drag results from the model tests of this investigation with faired values from large-scale flight tests showed good agreement, particularly at the higher tes Mach number of 3.0. Equivalent drag coefficients of the models were about 12 percent and 6 percent lower than faired flight results at Mach numbers 2.0 and 3.0, respectively. These comparative results indicate that small-scale tests similar to this investigation would be useful in the performance evaluation of large-scale decelerator systems.

INTRODUCTION

Langley Research Center has conducted extensive tests on aerodynamic decelerator in order to select a system suitable for supersonic deployment in low-density planetary atmospheres. Considerable effort has been devoted to supersonic flight tests of the disk-gap-band parachute configuration being considered for future missions to Mars. Some of these flight tests (refs. 1 to 3) consisted of a series of rocket launches with deployment over a Mach number range from 1.9 to 3.3 and at dynamic pressures from about 464 to 555 newtons per square meter. The flight-test parachutes had a nominal diameter of 12.19 meters and a geometric porosity of 12.5 percent. Results from the reference flight tests have shown that the disk-gap-band parachute developed poorly damped, high-amplitude oscillations in the drag loads because of instability of the canopy shape ("breathing") and elasticity in the suspension lines. One of the problems presented by these dynamic characteristics is in the extraction of a representative drag performance which could be used for comparison with competitive decelerator systems. Fairing of oscillatory force data could yield inconsistencies between results from comparable tests as shown in the summary report of reference 4.

In an effort to contribute additional experimental data on the oscillatory drag characteristics of the disk-gap-band parachute configuration at supersonic speeds, and in an attempt to correlate small-scale ground-test data with large-scale flight results, a wind-tunnel investigation of geometrically scaled models of the disk-gap-band parachute has been conducted by the Langley Research Center. Average nominal diameter of the parachute models was 1.65 meters with a reference geometric porosity of 12.5 percent.

The tests were performed in the 16-foot Supersonic Propulsion Wind Tunnel facility at the Arnold Engineering Development Center, Arnold Air Force Station, Tennessee, and were part of a comprehensive program for wind-tunnel tests of supersonic decelerators as described in references 5 and 6. The test parachutes were deployed and inflated over a Mach number range from 2.0 to 3.0 at a dynamic pressure of 3352 newtons per square meter (lowest available for this Mach number range). Other test variables included geometric porosity, attachment-point geometry and diameter, and suspension-line length. Some aspects of these tests have been previously reported in references 5 and 6. The purpose of this report is to present additional data and a more complete discussion of the results obtained from unreefed deployment of the disk-gap-band parachute models.

SYMBOLS

C_{D_o} drag coefficient based on nominal parachute area, $\frac{\text{Drag}}{qS_o}$

$C_{D_{o,av}}$ average drag coefficient from measurement frequency distribution, $\frac{1}{N}\sum_{i=1}^{N} N_i C_{D_{o,i}}$

$C_{D_{o,eq}}$ equivalent drag coefficient, $\frac{\sum C_{D_{o,av}}\, dt'}{t'}$

$C_{D_{o,i}}$ mean drag coefficient for an assigned range of values

D maximum diameter, meters

D_o nominal diameter of parachute canopy, meters

M free-stream Mach number

M_{av} average flight-test Mach number

N total number of samples

N_i number of drag-coefficient values within a range of values

q free-stream dynamic pressure, newtons/meter^2

S_o design nominal surface area of parachute including disk, gap, and band, meters^2

S_p projected area of canopy including vents and slots, meters^2

S_{p_o} projected area of canopy at first full inflation, meters^2

t time from deployment, seconds

t' time from first full inflation, seconds

X trailing distance between parachute canopy and attachment point on base extension, meters

α angle of attack of parachute canopy, degrees

β angle of sideslip of parachute canopy, degrees

η resultant angle of attack of parachute canopy, $\sqrt{\alpha^2 + \beta^2}$, degrees

λ_g geometric porosity, percent

Subscripts:

1 cylindrical base extension

2 conical base extension

TEST FACILITY AND APPARATUS

A complete description of the Propulsion Wind Tunnel facility employed for this investigation is given in reference 7. The test apparatus is illustrated by a sketch in figure 1 showing the forebody and base extension mounted on the test-section floor strut. Typical dimensions are shown with the test parachute deployed and inflated. The parachute was attached to the base of the extension through a riser, tensiometer with a swivel, and a three-leg bridle. A more detailed sketch of the forebody and base extension prior to deployment is shown in figure 2. The unique feature of this test apparatus was the

ability of the base extension to oscillate in either, or both, the pitch and yaw planes (no roll). This feature, incorporating a universal joint, was provided in an attempt to obtain a more realistic simulation of an oscillatory forebody wake during free flight. The maximum amplitude of the base-extension oscillations was 17.5°. The geometry of the base extension could be converted from the cylindrical configuration to a 120° conical configuration with the addition of an outer skirt. In both cases, the exposed face of the base extension was conical. Maximum cross-sectional diameter of the base extension was 15.2 cm for the cylindrical configuration and 30.48 cm for the conical configuration.

Prior to deployment, and during tunnel run-up to test conditions, the packaged decelerator was attached to the base extension and held against a deployment spring plate by three restraining straps. These straps were joined over the end of the bag by a line which passed through a pyrotechnic line cutter. In the loaded condition, the deployment spring plate was pulled up and held against the cylindrical section by a cable which was attached to an air cylinder in the sting. This arrangement also served to lock the base extension and prevent movement of the universal joint prior to deployment.

Deployment of the test parachute was accomplished by release of the restraining cable which permitted a spring-rod arrangement to expand against the base at 12 locations. Each spring, when fully compressed by the spring plate, exerted about 89 newtons of force against the spring plate. Upon release of the air pressure in the cylinder through a quick-acting solenoid valve, the stored spring force propelled the deployment spring plate rearward through a 2.03-cm stroke. Simultaneously, an electric current was supplied to initiate the pyrotechnic line cutter for release of the restraining straps holding the packaged parachute to the base plate. As also indicated in figure 2, the base extension was supported about the universal joint and air-seal section at the nose by structural members connected by flex beams which prevented lateral movement of the installation.

Referring back to figure 1, the ratio of canopy trailing distance to base-extension diameter was $X/D_1 = 13.4$ for the cylindrical base extension, and $X/D_2 = 6.7$ for the conical base extension. The trailing distance is taken as the distance between the leading edge of the canopy band and the bridle attachment point at the end of the base extension. Distance of spring-plate movement for deployment and inset of the conical skirt was not considered in these ratios.

Photographs of the test apparatus showing the variation in base-extension geometry are presented in figures 3, 4, and 5. The electrical leads to the pyrotechnic line cutter and the bridle attachment rings at the edge of the deployment spring plate are shown in figures 4(a) and 5(a), respectively. Figure 4(b) shows an installation of a packaged decelerator at the base of the conical section with the three restraining straps.

DESCRIPTION OF THE DISK-GAP-BAND PARACHUTE MODELS

Design Considerations

Detailed discussion of the design and construction of the disk-gap-band parachute models is presented in reference 8, a contractor report. The primary goal for design of the test parachutes was to achieve geometric similarity with the flight-test configuration having a nominal diameter of 12.19 meters and a basic geometric porosity of 12.5 percent. No attempt was made to establish structural scaling for dynamic similarity.

Based upon limitations imposed on model size by the wind-tunnel facilities, a design nominal diameter of 1.68 meters was selected for the test parachutes. The gore patterns of the models were established from the design procedures of reference 7, and the number of gores was selected to attain similarity between inflated profiles. Similarity to the full-scale geometry was maintained between ratios of disk gore height to gore width (at the gap) and between ratios of band gore height to gore width. These relationships were maintained by incorporating 32 gores for a geometric porosity of 12.5 percent.

In order to vary geometric porosity of the models from the basic value of 12.5 percent for the same nominal diameter, the disk geometry of the 12.5-percent design was held constant. The gap was decreased and the band correspondingly increased to derive a 10.0-percent geometric porosity, while the reverse was done to achieve a 15.0-percent geometric porosity. In order to retain approximately the same amount of open area at the vent as the 12.19-meter flight-test parachute, a vent diameter of 15.24 cm was required instead of a scaled value of 11.84 cm because of blockage from the radial tapes. In addition, it was necessary to fold the radial tapes as they crossed the vent in order to reduce their frontal area.

Construction Details

Figure 6 presents pertinent construction features of the parachute models used in this investigation. Emphasis was placed upon holding the variations between models to a minimum during the manufacturing process. An indication of the similarity actually achieved is shown in the table of figure 6. Variances in the nominal diameters of all the models fabricated were less than 3 cm, while the constructed disk diameters were within 1.40 cm. In addition, the gap widths and the band widths for each porosity did not vary more than 0.36 and 1.27 cm, respectively. The average of the nominal diameters of all of the test models was about 1.65 meters. Based upon this average, the ratio of canopy nominal diameter to base-extension diameter at the attachment point was about $D_o/D_1 = 11$ with the cylindrical base extension and about $D_o/D_2 = 5.5$ with the conical base extension.

The parachute models were constructed of dacron material weighing 76.3 grams per square meter. As indicated in figure 6, the assembly was comprised of 16 gores. An

additional 16 meridional tapes were used to divide the 16 gores in an attempt to simulate the inflated shape of the full-scale parachute having 32 gores with 32 suspension lines. The band was constructed from one piece of fabric with the warp at 45° to the meridional tape. A photograph of the completed parachute is shown in figure 7.

INSTRUMENTATION AND DATA REDUCTION

As shown previously in figures 1 and 2, a load cell was used to measure total drag forces of the parachute model plus forebody, and a tensiometer with swivel was used to measure drag forces of the parachute system alone. The load cell had a capacity of 8900 newtons and measured forebody drag prior to deployment of the parachute. The tensiometer had a capacity of 8000 newtons. Force measurements from the load cell and tensiometer were estimated to be accurate within ± 44.5 newtons. Outputs from both the load cell and tensiometer were continuously recorded on oscillographs and were also digitized and recorded on magnetic tape for instantaneous data reduction. Four 16-mm motion-picture cameras were positioned in the wind-tunnel walls to document deployment and inflation characteristics of the test parachutes from top, both sides, and downstream.

The average drag coefficients of the parachute models were computed from the tensiometer and load-cell force measurements using a statistical program as described in reference 6. The average drag coefficients derived from the load-cell measurements will be presented with forebody drag removed. No attempt was made to estimate the effects of friction of the oscillating base extension on the computed drag coefficients. The statistical calculations of reference 6, using load-cell and tensiometer measurements sampled at a rate of 1000 samples per second, were averaged over a 1-second interval at about every 3 to 4 seconds. The data were grouped into a finite number of cells that covered the range of drag-coefficient values recorded by the digital data recording system. Each cell was assigned a given range of drag-coefficient values and a mean drag-coefficient value that was the average of that range. The average value from this frequency distribution then represented the most probable value of the drag coefficient for each sample. Since the average drag coefficients varied over the test time interval, an additional calculation was made to obtain a representative constant drag coefficient for each test interval. This value is defined and presented herein as the equivalent drag coefficient. Comparison between equivalent drag coefficients derived from load-cell and tensiometer measurements indicated that the values from these two sources were usually within 2 percent.

The projected inflation area of the parachute canopy was measured from the motion-picture film data and reference grid boards recorded by the downstream camera. The film data were also used to derive attitude angles of the parachute canopy with respect to the stationary forebody located near the center line of the tunnel. These angles were

obtained as angle of attack α in the vertical plane, sideslip angle β in the horizontal plane, and the resultant angle η. The time reference for the canopy attitude angles and projected inflation areas was correlated with the initial peak forces measured by the tensiometer and load cell.

RESULTS AND DISCUSSION

Drag Force Measurements

Typical supersonic characteristics of the parachute models during deployment and inflation are illustrated by sequence photographs in figure 8. As seen in figures 8(f) to 8(h), the parachute canopy experienced periodic partial collapse and reinflation (breathing) in a manner similar to that exhibited by the full-scale flight parachutes. These variations in canopy shape were accompanied by oscillations in the suspension lines which produced high-frequency, oscillatory drag forces as shown in figures 9 and 10. Referring to figure 9, small differences can be noted between the frequencies of the tensiometer and load-cell measurements. Comparison of these measurements in figure 10 shows that there were also differences in amplitudes of the drag forces. The load-cell measurements, influenced by oscillations of the flexible-floor strut coupled with inertia of the forebody, recorded maximum and minimum values (negative in some cases) which were greater than the peak forces produced by the parachute system recorded by the tensiometer. Average levels of the forces from load-cell measurements, however, appeared to be compatible with averages of the tensiometer measurements and were used either to confirm average drag values derived from the tensiometer or to obtain averages in the absence of tensiometer data.

It should be noted that time histories of the oscillatory forces obtained from these tests could not be expected to duplicate full-scale flight results, since dynamic scaling of the parachute model was not attempted. Although the spring-mass systems were different, it was expected that instability of the model canopy shape (breathing) would produce average oscillatory drag forces similar in amplitude but increased in frequency by the inverse of the nominal-diameter ratios. Averages of these model drag forces over a period of time, then, should yield an equivalent drag performance which could be correlated with averages from full-scale flight results.

Canopy Motion and Inflation Characteristics

The dynamic behavior of the test parachute at Mach numbers 2.0 and 3.0 is illustrated in figures 11 and 12. This example is for the parachute model tested with a geometric porosity of 12.5 percent and the cylindrical base extension. Comparison of the time histories of the tensiometer force measurements with the canopy projected-area ratios in figure 11 indicated that these tests with the cylindrical base extension yielded

low-frequency variations in canopy areas which produced corresponding low-frequency force data similar to the flight measurements. This correlation is evident during the initial cycles of breathing where it can be seen that the low-frequency tensiometer forces peaked at about the same time the canopy projected areas reached a maximum. Canopy attitude angles appeared to have little direct influence on the tensiometer force measurements. The influence of canopy inflation areas on the load-cell measurements was difficult to determine, since the low-frequency longitudinal forces recorded by the load cell appeared to be dependent on both the inflation areas and the attitude angles of the canopy.

The effect of increasing the test Mach number from 2.0 to 3.0 on the dynamic characteristics of the parachute model is indicated by the comparison between results of figures 11 and 12. Higher-amplitude fluctuations in canopy attitude angles, accompanied by larger variations in canopy projected areas, were exhibited during this test at the higher Mach number. It should be noted that the average projected area of the canopy and drag level at Mach number 3.0 was smaller, and the initial projected area S_{p_o} was only 86 percent of the area at a Mach number of 2.0.

An attempt was made to determine if there was any relationship between the oscillatory attitude angles of the parachute canopy and the projected drag areas produced by the canopy. Time histories of α and β showed that the canopy experienced both planar and conical motions which appeared to diverge intermittently with time. The maximum resultant angle of attack during these tests was about 15°. During these angular oscillations, no correlation between angles of attack of the parachute canopy and the projected drag areas could be found, since collapse and reinflation of the canopy occurred at random angles of attack.

As seen in figure 13, the frequency of the inflation cycles also appeared to be independent of the motion frequencies at both test Mach numbers of 2.0 and 3.0 and with both the cylindrical and conical base extension. These results indicated that the model canopy breathing frequency was not constant, but varied by about 15 cycles per second over the test period. The frequency of one inflation cycle during rocket-launch tests of the full-scale parachute is superimposed in figure 13 for average flight-test Mach numbers near those for the model tests. These full-scale frequencies are shown to scale up (nominal diameters of the test parachutes) to an approximate average frequency exhibited by the models at a test Mach number of 3.0 with the cylindrical base extension. At the lower Mach number of 2.0, average frequencies of canopy breathing from the model tests were lower than the scaled flight frequencies.

Effect of geometric porosity.- Changes in geometric porosity of the test parachutes produced variations in canopy inflation and angles of attack as illustrated in figure 14 for a test Mach number of 2.0 with the cylindrical base extension. Comparison of these data did not reveal any obvious trends in the oscillatory characteristics of either the angles of

attack or the projected-area ratios as geometric porosity was changed. One effect of the change in geometric porosity was that the projected area of the canopy at first full inflation decreased as the geometric porosity was varied about the basic value of 12.5 percent (see initial projected-area comparison in fig. 14).

Addition of conical skirt.- Inflation and motion characteristics of the test parachutes are compared in figure 15 for deployment and inflation behind the cylindrical and conical base extensions. These data are for a geometric porosity of 12.5 percent and showed that a change in base extension resulted in a significant difference between the projected-area ratios and between the oscillatory motions. At a test Mach number of 2.0, the size of the canopy projected area at initial inflation behind the cylindrical base extension was reduced by about 12 percent with the addition of the conical skirt. At the high Mach number of 3.0, this reduction was more pronounced at 20 percent. Although the projected drag areas of the canopy were smaller with the conical base extension at both test Mach numbers, the addition of the conical skirt appeared to alleviate the fluctuations in canopy inflation and motions, especially at the higher test Mach number of 3.0.

Effect of suspension-line length.- Figure 16 presents sequence photographs obtained during a test conducted at Mach number 2.5 with the suspension lines increased from $X/D_2 = 6.7$ to $X/D_2 = 9.6$ behind the conical base extension. Geometric porosity of the parachute model for this investigation was 12.5 percent. Figure 17 presents the time histories of angles of attack and inflation characteristics with the longer suspension lines. Although not shown, the projected inflation area of the canopy at Mach number 2.5 was larger than the areas produced at either Mach number 2.0 or 3.0 with the shorter suspension lines. Comparison of the sequence photographs in figure 16 with other data for the shorter suspension lines, however, indicated that the profile shapes of the canopy with the longer suspension lines were more irregular with pronounced flattening and elongation. In addition, angle-of-attack comparisons as shown in figure 17 revealed a significant increase in canopy angles of attack with the longer suspension lines.

Parachute Drag Performance

For comparative purposes, equivalent drag coefficients will be used to show the change in parachute drag performance with change in the test variables. These drag values will also be used for correlation with flight-test results. In addition, equivalent drag coefficients derived from the load cell and from the tensiometer are compared when both data sources are available.

Effect of geometric porosity.- Figures 18 through 20 present time histories of the average drag coefficients, and corresponding equivalent drag coefficients, at Mach numbers from 2.0 to 3.0 for the range of geometric porosities tested. These data were obtained with deployment and inflation behind the cylindrical base extension. Only one

data point was obtained at a Mach number of 3.0 for a geometric porosity of 12.5 percent. The parachute model with a geometric porosity of 12.5 percent was not tested at Mach number 2.5.

Comparison of the equivalent drag coefficients from tensiometer measurements with those from load-cell measurements in figures 18 and 19 shows that good agreement was obtained between the two measurements. For the repeat tests of figure 18(c), comparison of equivalent drag coefficients indicated questionable results from one set of tensiometer measurements. The tensiometer later failed and was replaced.

A summary fairing showing the variations of equivalent drag coefficients with changes in geometric porosity and Mach number is presented in figure 21. These data showed that effect of changes in geometric porosity on drag performance was small for the range of porosities tested.

Addition of conical skirt and suspension-line length.- Figure 22 presents average and equivalent drag coefficients for the parachutes tested with 12.5-percent geometric porosity and the conical skirt installed $\left(X/D_2 = 6.7\right)$. No tensiometer measurements were recorded during these tests. The data of figures 22(b) and 22(c) were obtained at Mach numbers of 2.25 and 2.5 with the base extension inadvertently locked and unable to oscillate. Figure 23 shows values of average and equivalent drag coefficients for a test conducted at a Mach number of 2.5 with the suspension lines increased to give an $X/D_2 = 9.6$. The data were also collected with the conical skirt installed and with a geometric porosity of 12.5 percent.

The summary plot of faired data presented in figure 24 indicated that the addition of the conical skirt with the shorter suspension lines at $X/D_2 = 6.7$ resulted in a reduction in equivalent drag coefficient of about 2 percent. Increasing the length of the suspension lines to $X/D_2 = 9.6$, however, resulted in an increase in equivalent drag of about 30 percent at a Mach number of 2.5. As previously mentioned, this improvement in drag performance with longer suspension lines was accompanied by higher amplitude and higher frequency motions at the canopy. In addition, fluctuations in canopy profile shape became more pronounced with the longer suspension lines.

Comparison with flight-test results.- Figure 25 presents a comparison between the equivalent drag coefficients from this investigation with the oscillatory drag obtained from flight tests of the large-scale disk-gap-band parachute (refs. 1 to 3). The flight parachute had a nominal diameter of 12.19 meters and a geometric porosity of 12.5 percent. The equivalent drag coefficients shown for the model tests are also for models with a geometric porosity of 12.5 percent and with the cylindrical base extension. The inset illustration in figure 25 shows the geometric differences between the model and large-scale systems.

Comparison of the model data with fairing of the oscillatory flight results (as given in the summary report, ref. 4) showed good agreement, particularly at the higher test

Mach number of 3.0. This comparison indicated that the equivalent drag produced by the models of this investigation was about 12 percent and 6 percent lower than the faired flight values at Mach numbers 2.0 and 3.0, respectively. Part of these differences may have been caused by differences in the wake flows, dynamic pressures, transient flow fields from decelerating flight, or fairing of the oscillatory flight data.

Although the individual effects on drag caused by differences between the model and large-scale flight environment could not be isolated, it is believed that the comparative results of figure 25 show that small-scale ground tests would be useful for performance evaluation of large-scale decelerator systems.

SUMMARY OF RESULTS

A wind-tunnel investigation of the oscillatory drag characteristics of a disk-gap-band parachute with an average nominal diameter of 1.65 meters has been conducted at Mach numbers from 2.0 to 3.0 and at a dynamic pressure of 3352 newtons per square meter. Analysis of drag-force measurements and motion-picture data obtained during these tests have indicated the following results:

1. The test parachutes exhibited low-frequency variations in canopy projected areas ("breathing") which were similar in amplitude to large-scale flight results, but were increased in frequency by the inverse of the diameter ratios. The low-frequency changes in canopy areas also produced low-frequency, average drag data similar in character to flight measurements.

2. The magnitude and frequency of canopy breathing did not appear to be influenced by the attitude angles of the canopy up to a maximum resultant angle of attack of about 17.5°.

3. As the test Mach number was increased from 2.0 to 3.0, the variations in projected areas of the canopy became more pronounced.

4. Tests with geometric porosities of 10.0, 12.5, and 15.0 percent over the Mach number range from 2.0 to 3.0 did not reveal any significant differences in drag performance of the parachute models. In addition, no obvious trends for the differences in canopy motions and inflation characteristics could be found for this range of geometric porosities.

5. The addition of a conical skirt which changed the base-extension geometry from a cylindrical configuration $\left(X/D_1 = 13.4\right)$ to a conical configuration $\left(X/D_2 = 6.7\right)$ resulted in a reduction in projected area of the canopy of about 12 percent and 20 percent at Mach numbers from 2.0 to 3.0, respectively. These results showed a corresponding reduction

in equivalent drag coefficient of about 5 percent over the same Mach number range. Deployment behind the conical base extension, however, appeared to alleviate the fluctuations in canopy inflation and angles of attack, particularly at the higher test Mach number of 3.0.

6. An increase in suspension-line length, with a corresponding increase in canopy trailing distance from $X/D_2 = 6.7$ to $X/D_2 = 9.6$ behind the conical base extension, resulted in an increase in equivalent drag coefficient of about 30 percent at a Mach number of 2.5. This improvement in parachute drag performance, however, was accompanied by pronounced fluctuations in canopy profile shape and a significant increase in canopy angles of attack.

7. Good agreement was obtained between equivalent drag performance from these model tests with averages of oscillatory drag from large-scale flight results. Equivalent drag from the model tests was about 12 percent and 6 percent lower than fairing of the oscillatory flight data at Mach numbers from 2.0 to 3.0, respectively. Although these differences could not be isolated, it is believed that results from small-scale tests similar to this investigation would be useful for performance evaluation of large-scale decelerator systems.

Langley Research Center,
National Aeronautics and Space Administration,
Hampton, Va., September 14, 1972.

REFERENCES

1. Preisser, John S.; and Eckstrom, Clinton V.: Flight Test of a 40-Foot-Nominal-Diameter Disk-Gap-Band Parachute Deployed at a Mach Number of 1.91 and a Dynamic Pressure of 11.6 Pounds Per Square Foot. NASA TM X-1575, 1968.

2. Eckstrom, Clinton V.; and Preisser, John S.: Flight Test of a 40-Foot-Nominal-Diameter Disk-Gap-Band Parachute Deployed at a Mach Number of 2.72 and a Dynamic Pressure of 9.7 Pounds Per Square Foot. NASA TM X-1623, 1968.

3. Eckstrom, Clinton V.: Flight Test of a 40-Foot-Nominal-Diameter Disk-Gap-Band Parachute Deployed at a Mach Number of 3.31 and a Dynamic Pressure of 10.6 Pounds Per Square Foot. NASA TM X-1924, 1970.

4. Whitlock, Charles H.; and Bendura, Richard J.: Inflation and Performance of Three Parachute Configurations From Supersonic Flight Tests in a Low-Density Environment. NASA TN D-5296, 1969.

5. Bobbitt, P. J.; Mayhue, R. J.; Faurote, G. L.; and Galigher, L. L.: Supersonic and Subsonic Wind-Tunnel Tests of Reefed and Unreefed Disk-Gap-Band Parachutes. AIAA Paper No. 70-1172, Sept. 1970.

6. Galigher, Lawrence L.: Aerodynamic Characteristics of Ballutes and Disk-Gap-Band Parachutes at Mach Numbers From 1.8 to 3.7. AEDC-TR-69-245, U.S. Air Force, Nov. 1969. (Available from DDC as AD 861 437.)

7. Anon.: Test Facilities Handbook. Sixth ed., Arnold Eng. Develop. Center, Nov. 1966. (Available from DDC as AD 803 822.)

8. Faurote, G. L.: Design of Disk-Gap-Band and Modified Ringsail Parachutes and Development of Ballute Apex Inlet for Supersonic Application. GER-14657 (Contract NAS 1-8564), Goodyear Aerospace Corp., Apr. 6, 1970. (Available as NASA CR-66909.)

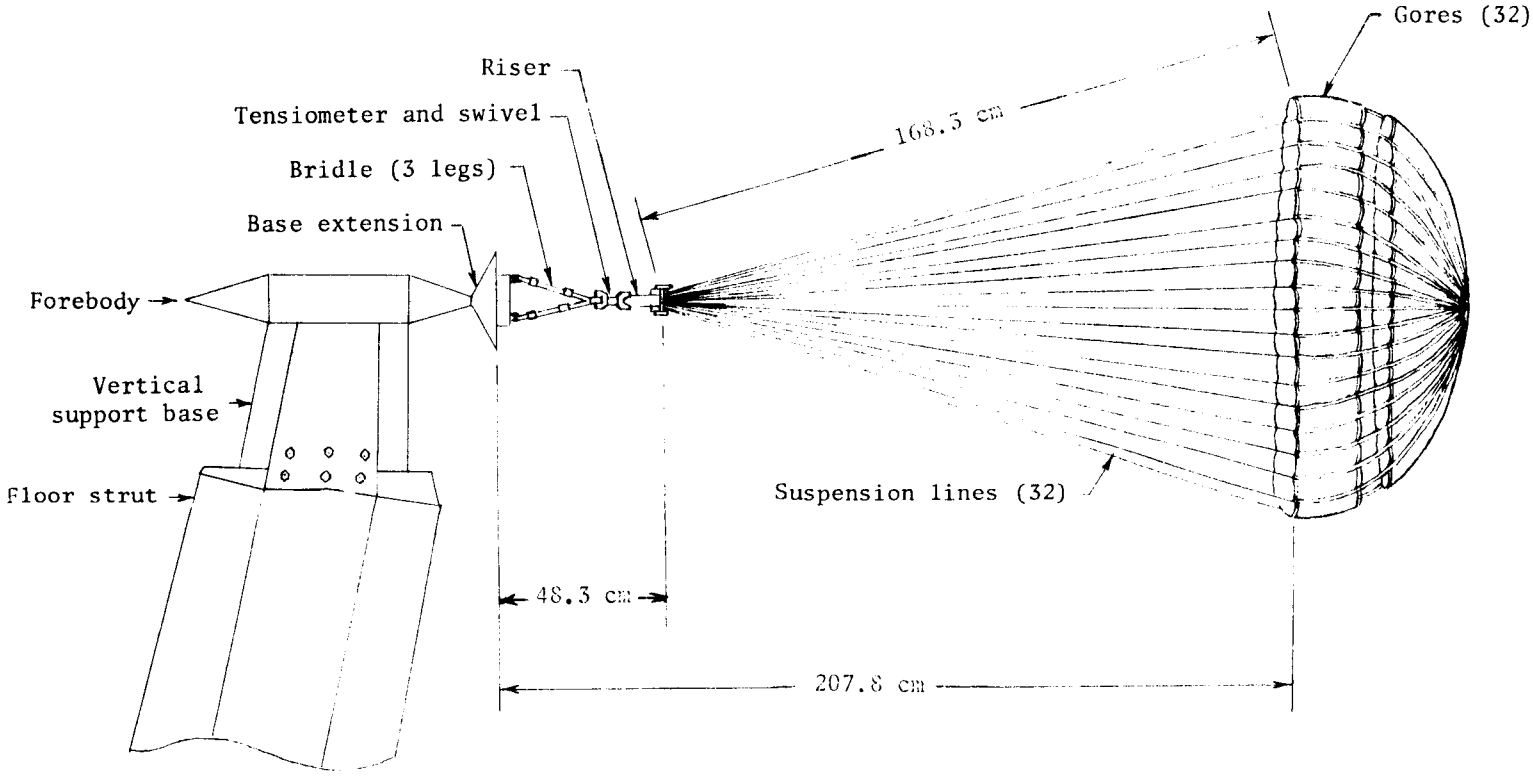

Figure 1.- Typical test configuration after parachute deployment.

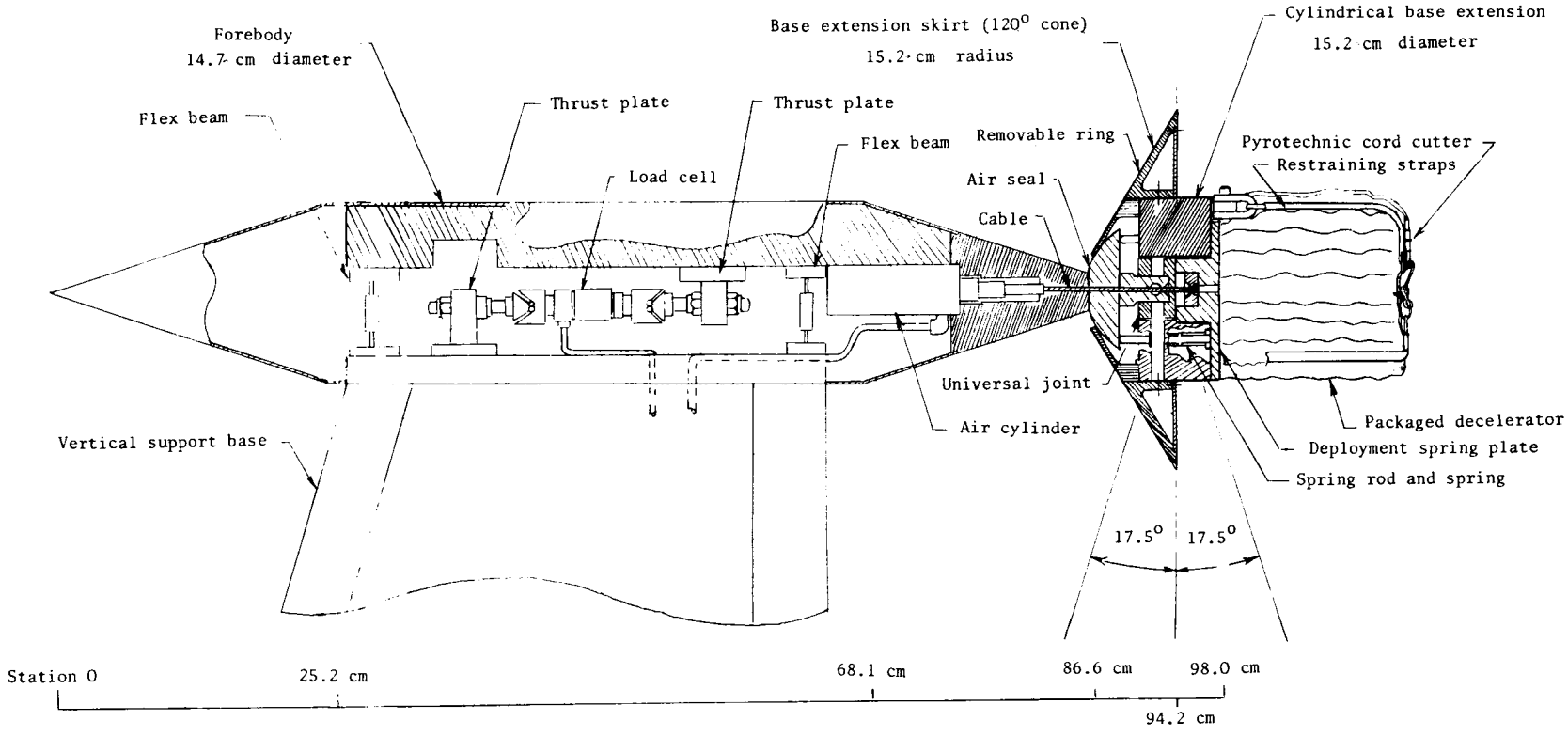

Figure 2.- Cross-sectional view of test configuration.

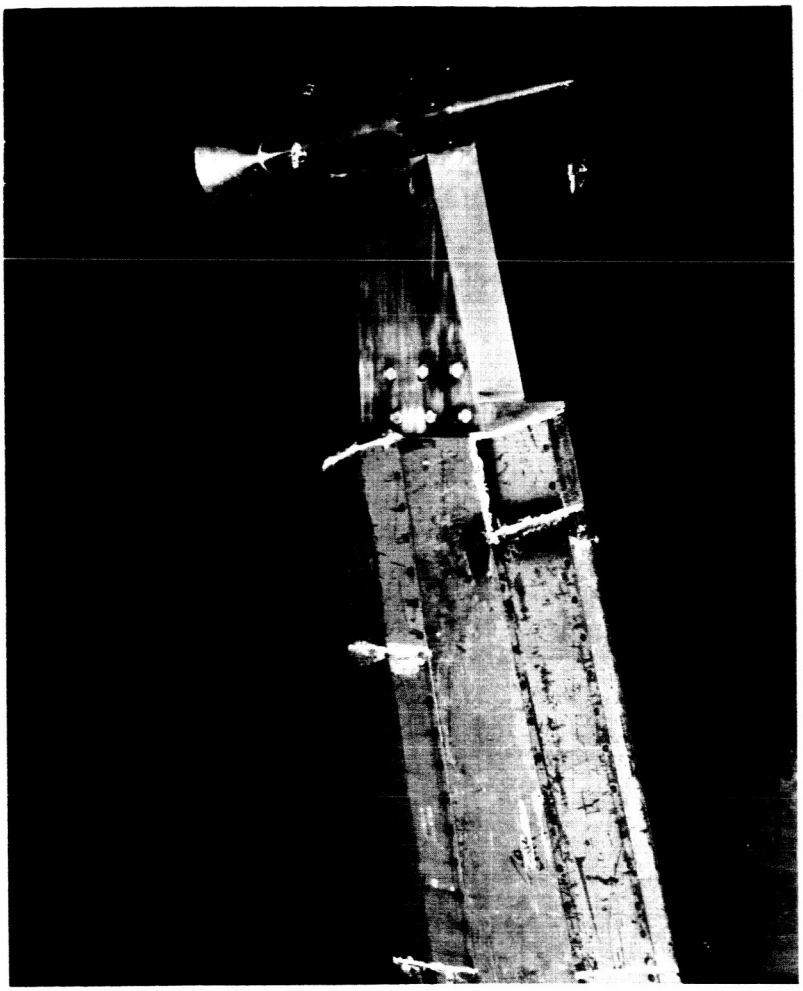

L-72-2495

Figure 3.- Front quarter view of forebody strut with conical base extension.

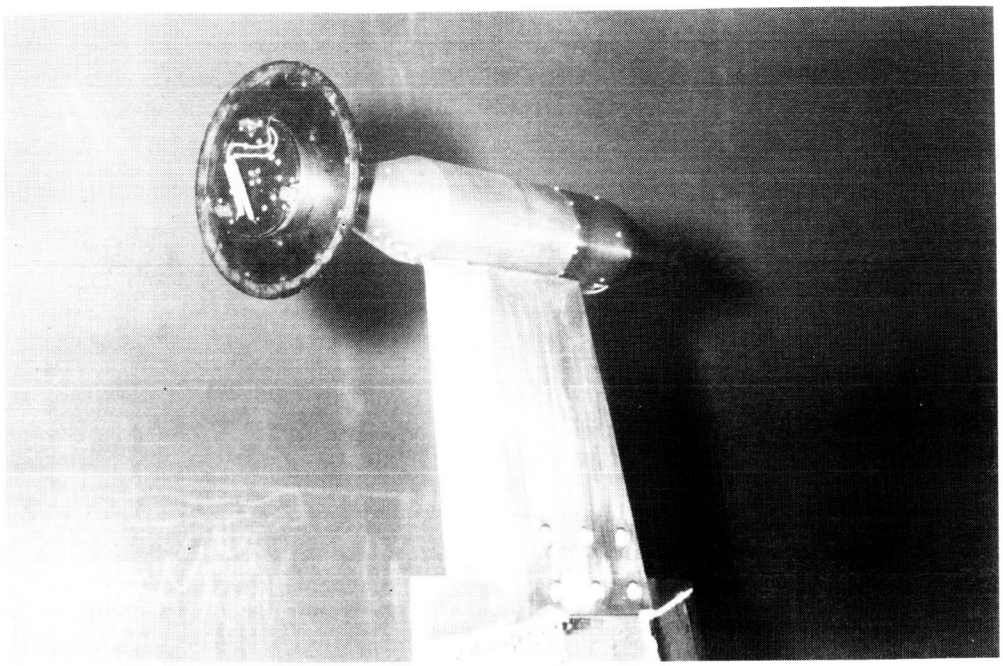

(a) Without decelerator.

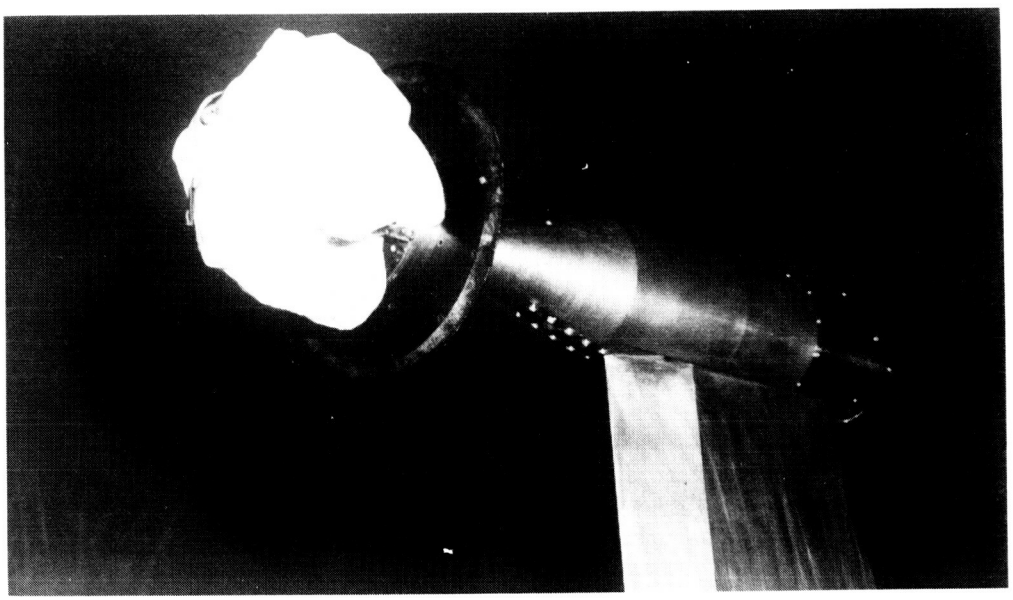

L-72-2496

(b) Decelerator installed.

Figure 4.- Rear quarter view of conical base extension.

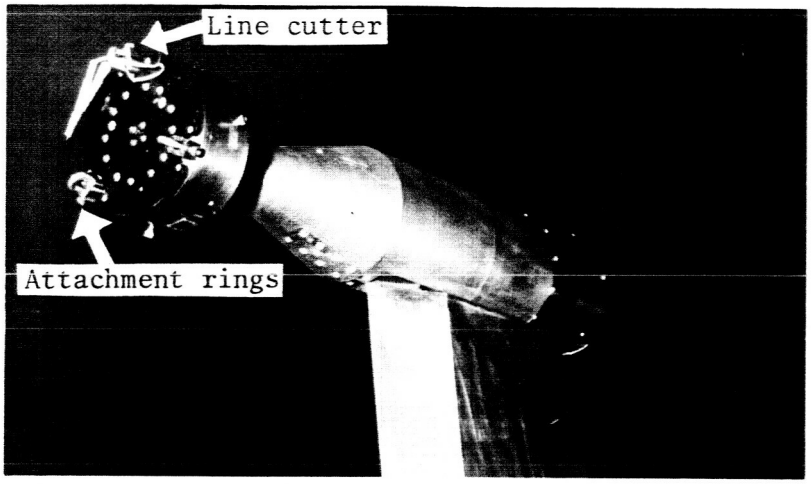

(a) Rear view.

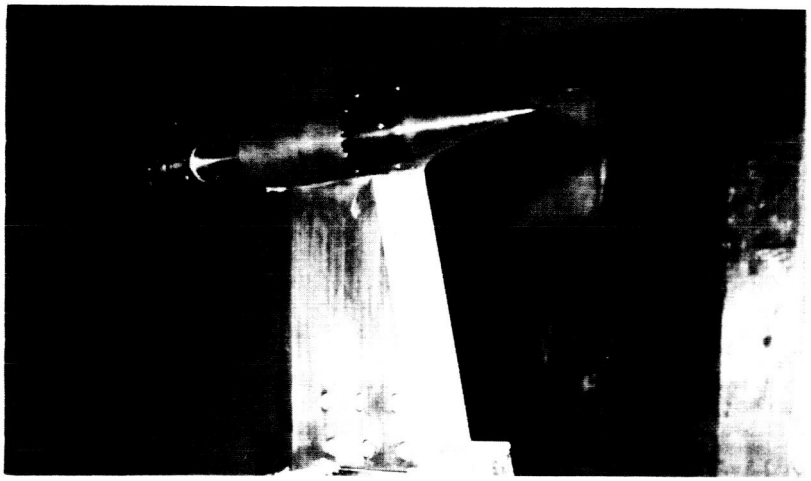

L-72-2497

(b) Front view.

Figure 5.- Forebody with cylindrical base extension.

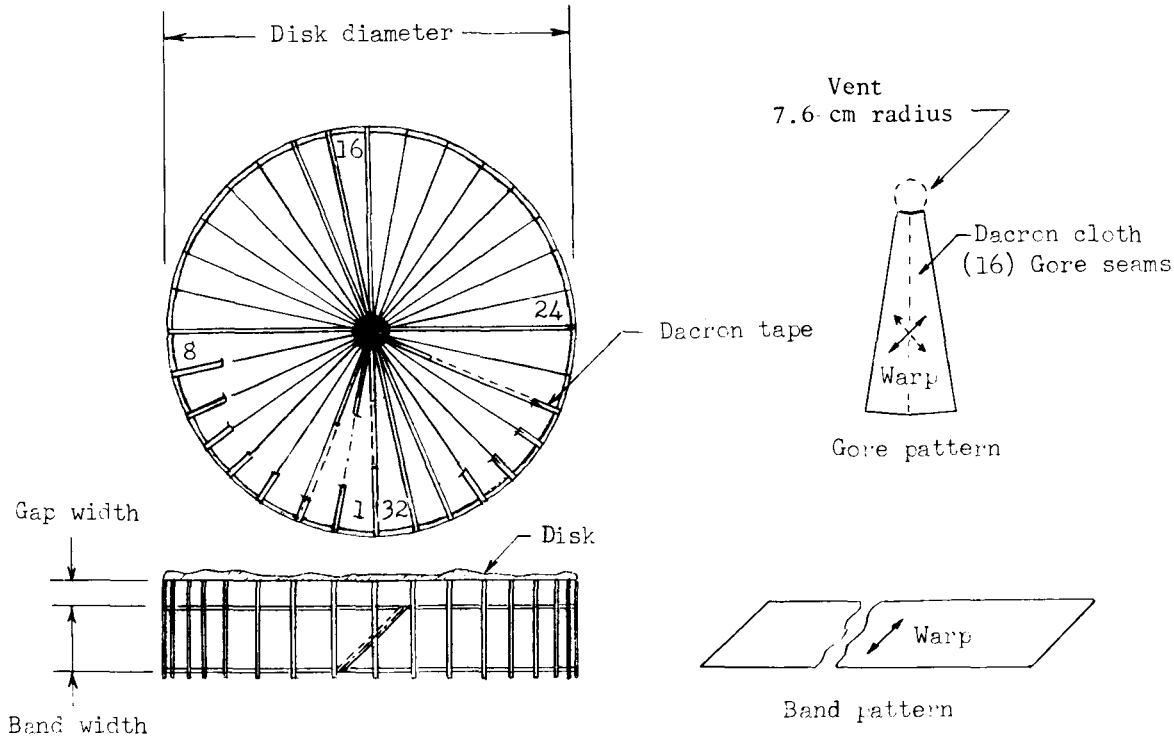

Model Number	Geometric porosity (percent)	Disk diameter (cm)	Gap width (cm)	Band width (cm)	Measured D_o (m)
1	12.5	120.37	6.81	19.25	1.643
2		120.65	6.73	19.53	1.649
3		120.37	6.83	19.18	1.643
4		119.71	6.96	19.48	1.640
5		120.52	6.68	20.17	1.649
6		119.96	6.76	19.00	1.637
7	10.0	119.99	5.44	20.57	1.643
8		119.25	5.61	20.68	1.661
9		120.14	5.69	20.52	1.643
10	15.0	119.86	8.51	18.26	1.649
11		120.29	8.38	19.53	1.667
12		120.52	8.15	18.69	1.655

Figure 6.- Construction features and dimensions of disk-gap-band parachute models.

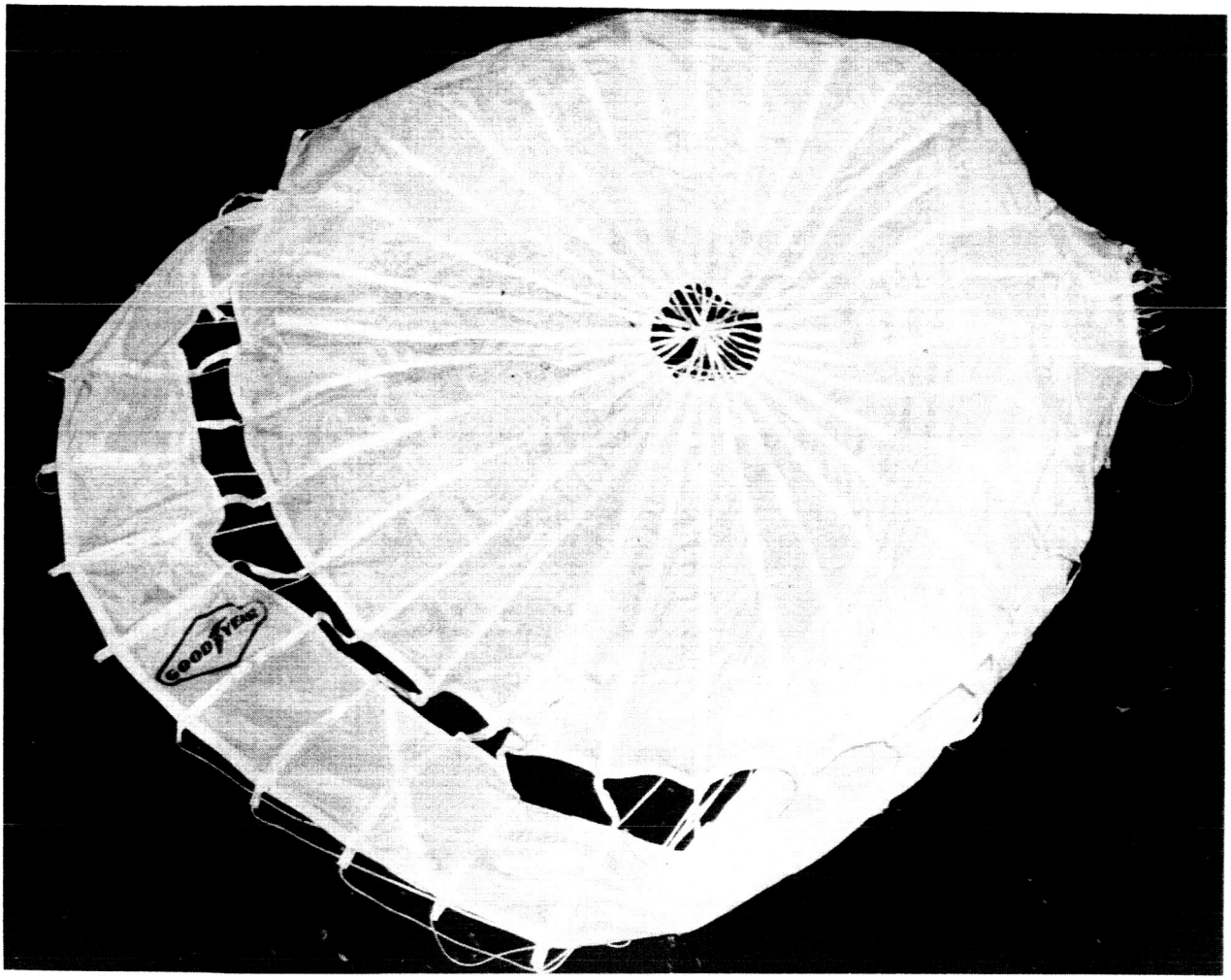

L-72-2498

Figure 7.- Disk-gap-band parachute model.

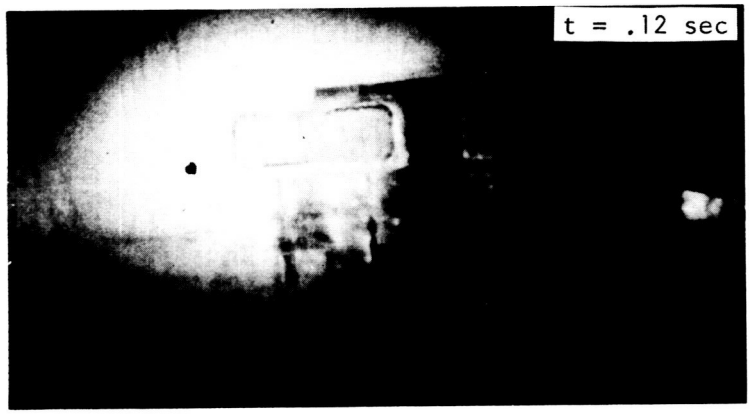

(a) Deployment.

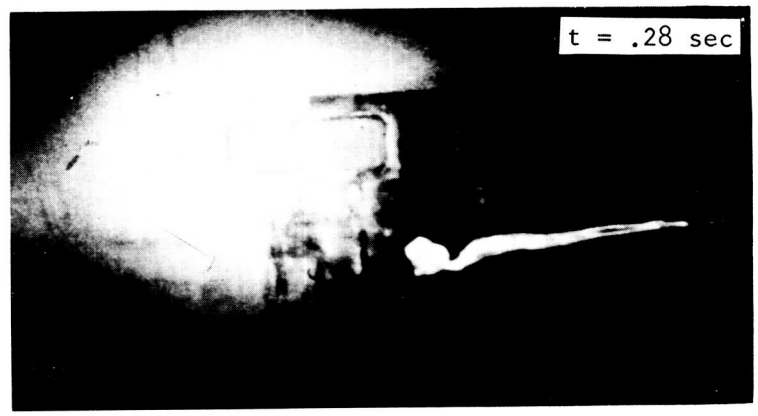

(b) Line strip.

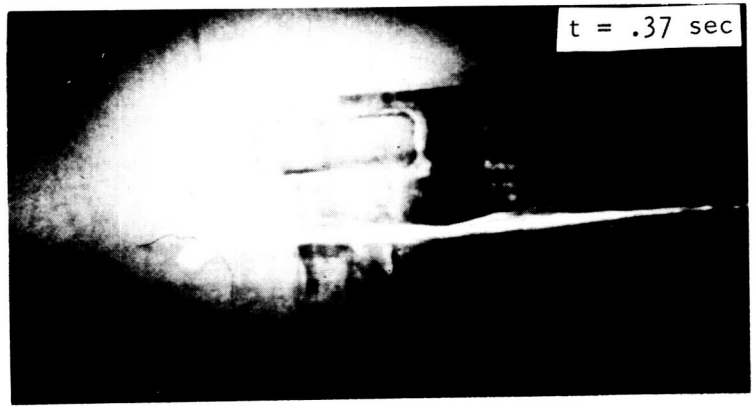

(c) Line stretch.

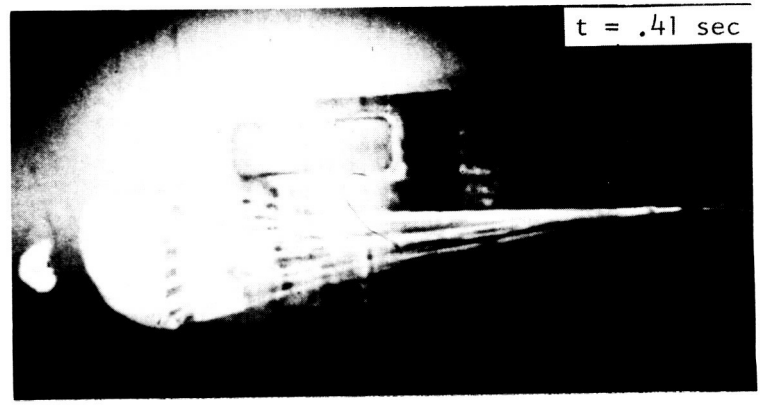

L-72-2499

(d) Bag strip and partial inflation.

Figure 8.- Sequence photographs of a typical deployment and inflation of test parachutes.

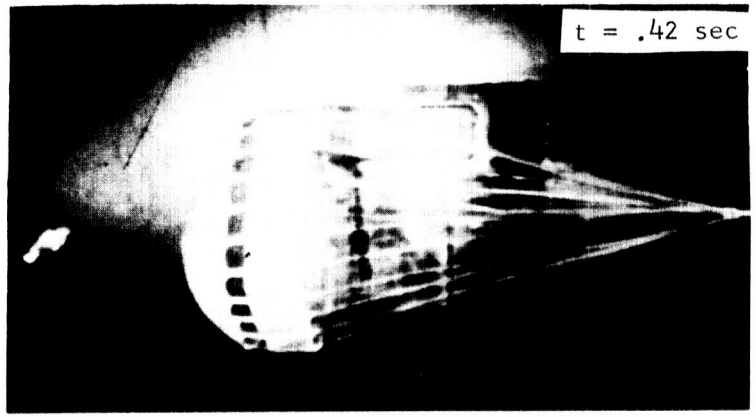

(e) Filling.

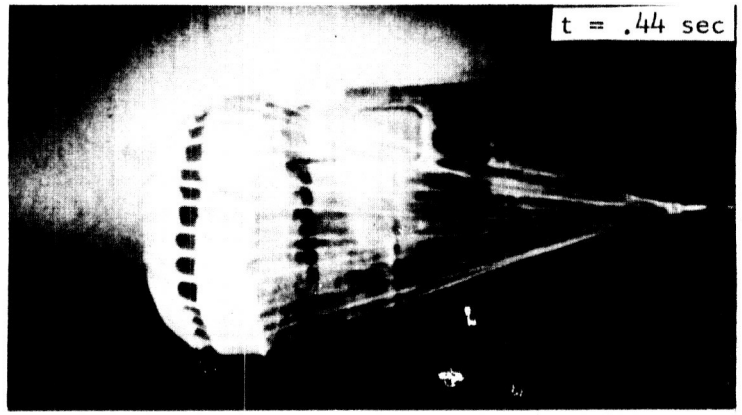

(f) Inflation.

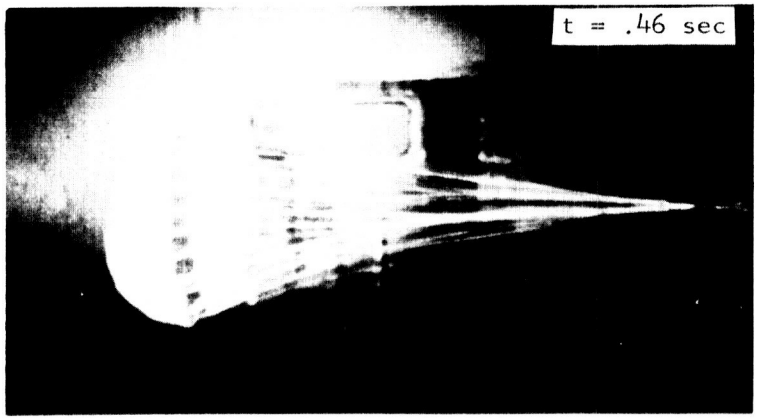

(g) Collapse.

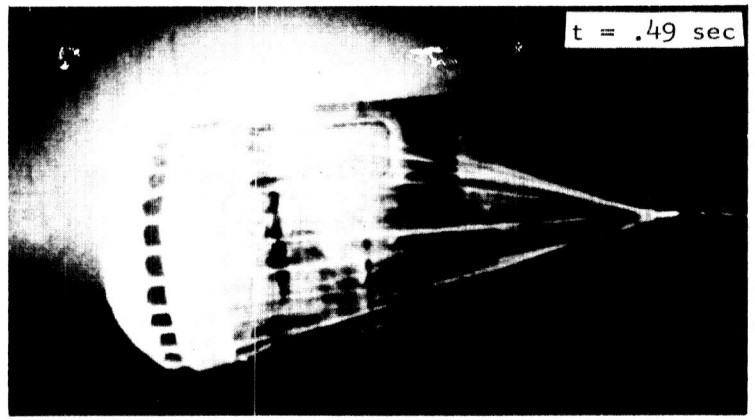

L-72-2500

(h) Reinflation.

Figure 8.- Concluded.

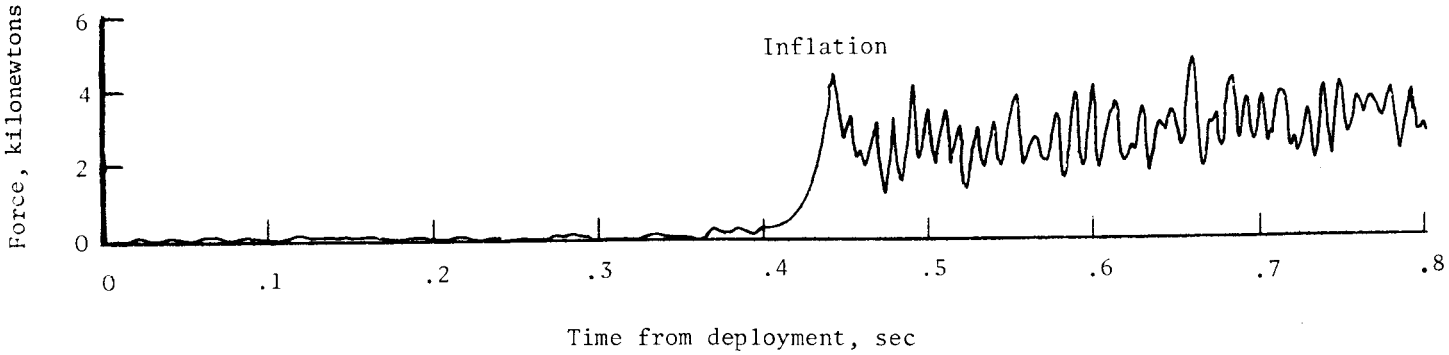

(a) Tensiometer measurements.

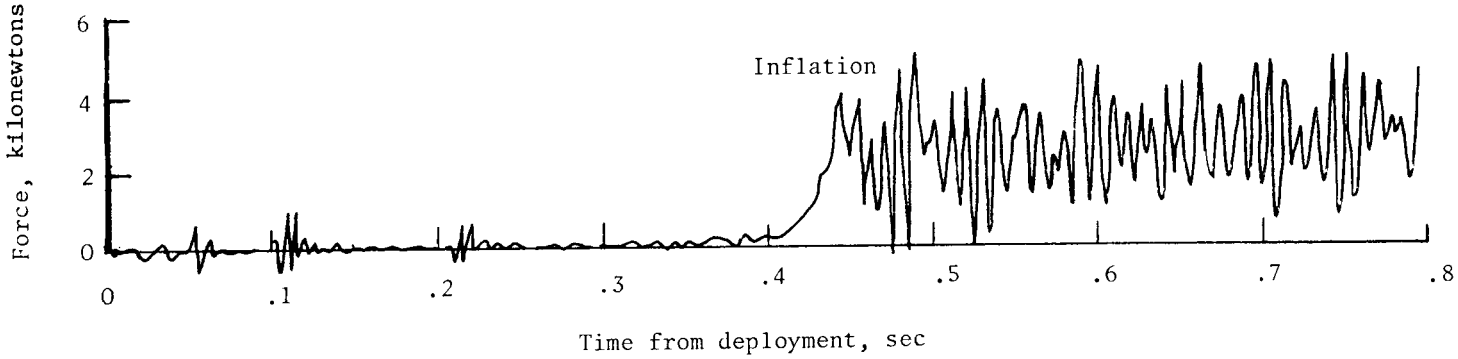

(b) Load-cell measurements.

Figure 9.- Typical time histories of drag-force measurements with cylindrical base extension at $M = 2.0$.

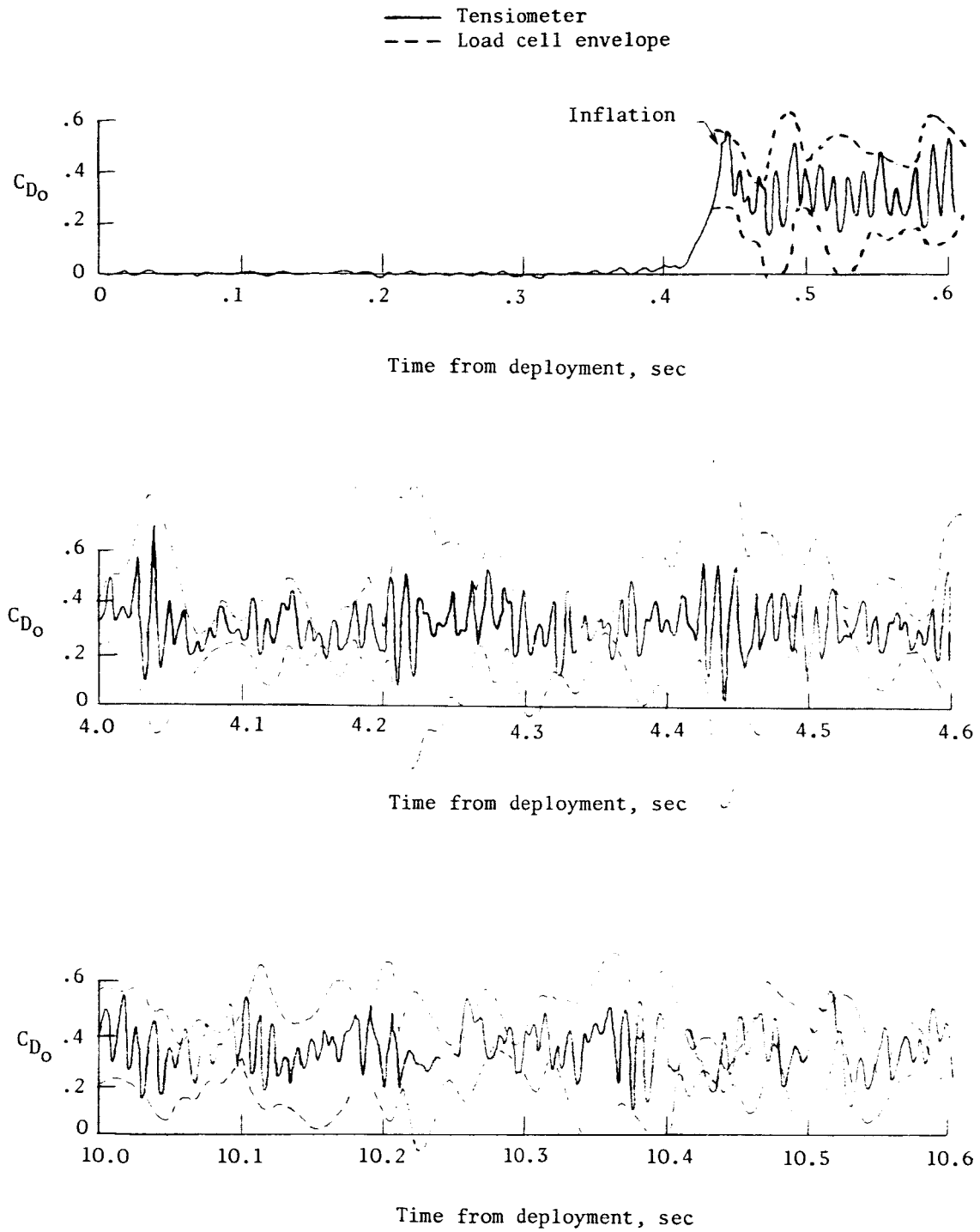

Figure 10.- Time histories of drag coefficients at M = 2.0 for 12.5-percent geometric porosity model behind cylindrical base extension for three different periods during a test.

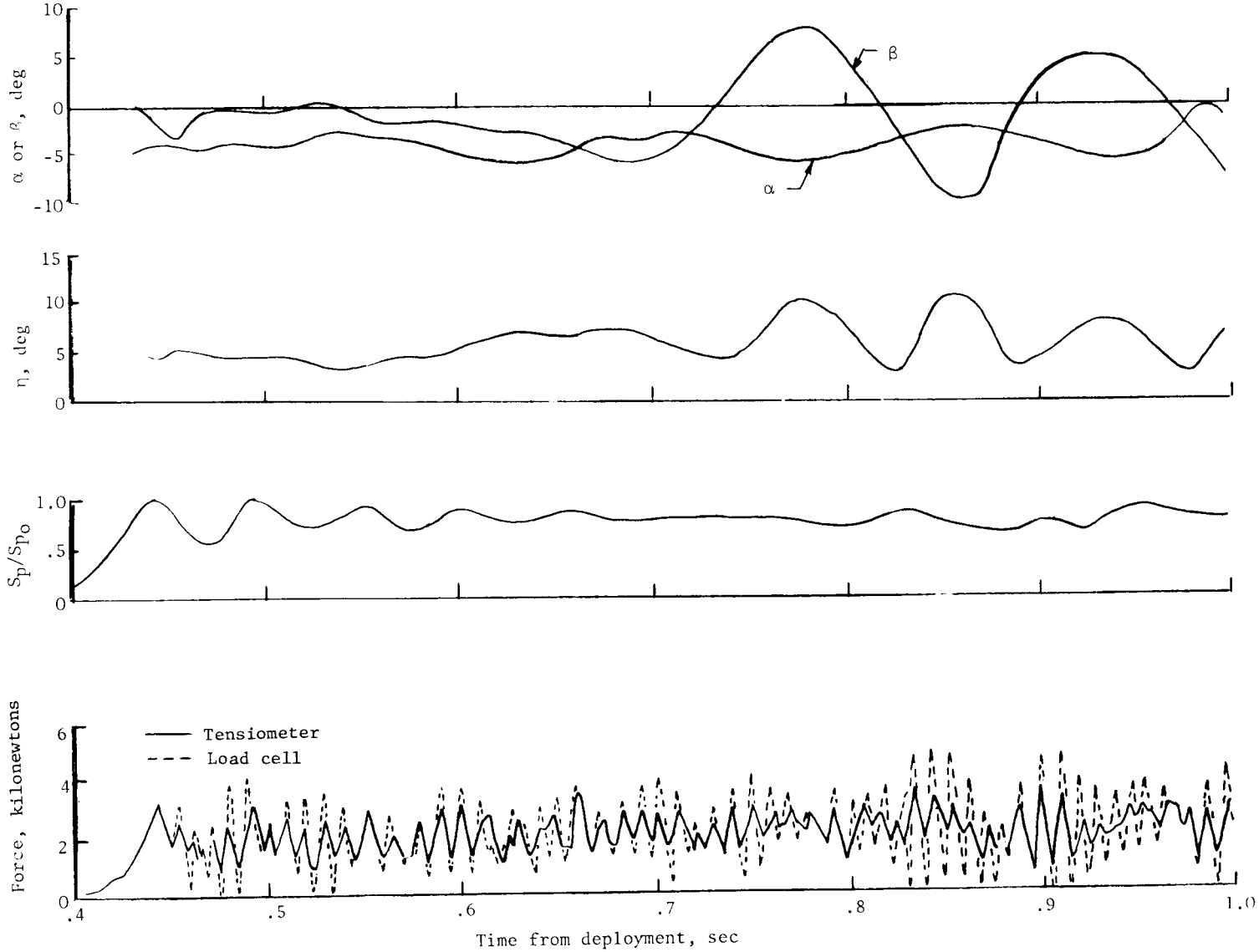

Figure 11.- Dynamic characteristics at M = 2.0 with cylindrical base extension (λ_g = 12.5 percent).

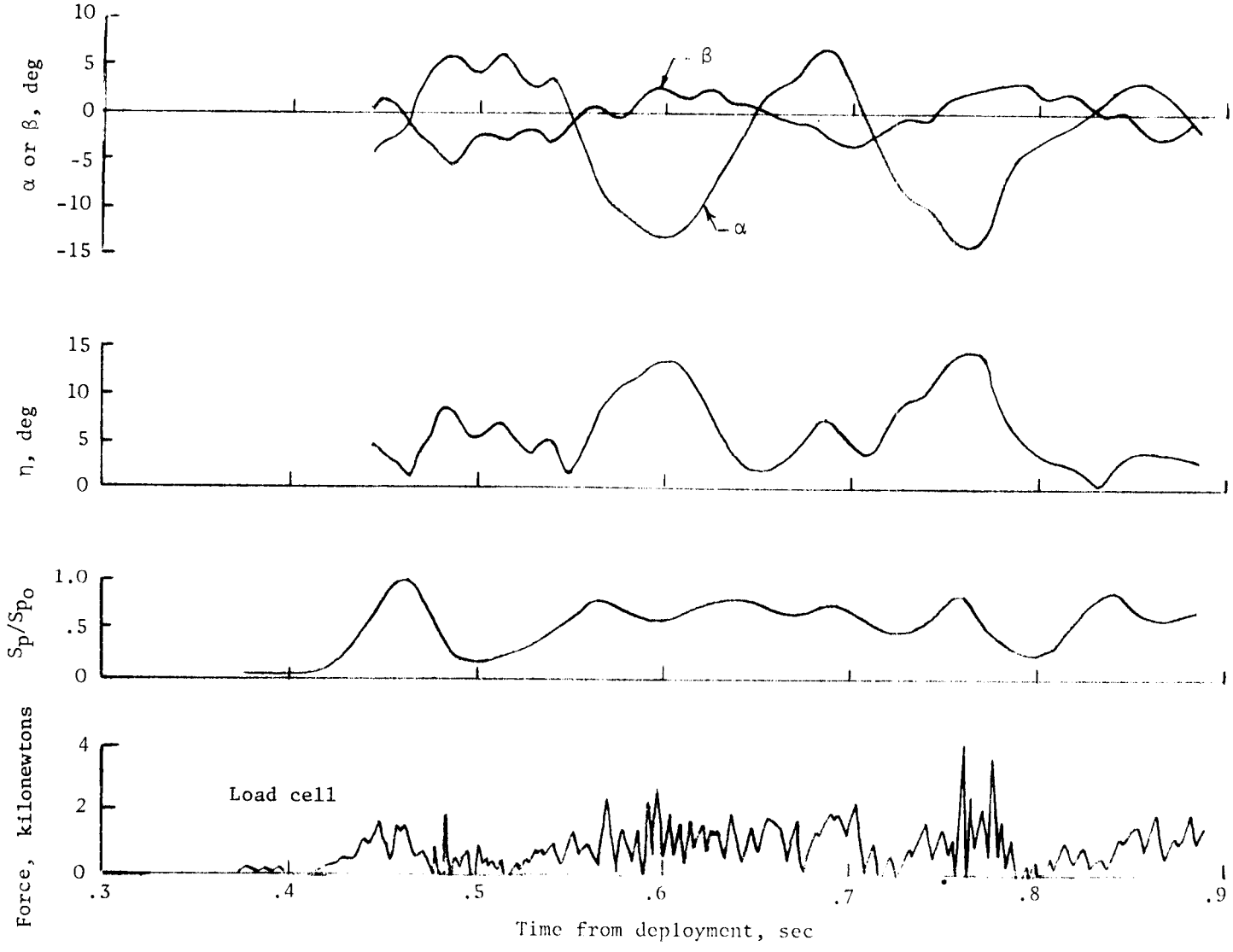

Figure 12.- Dynamic characteristics at M = 3.0 with cylindrical base extension (λ_g = 12.5 percent).

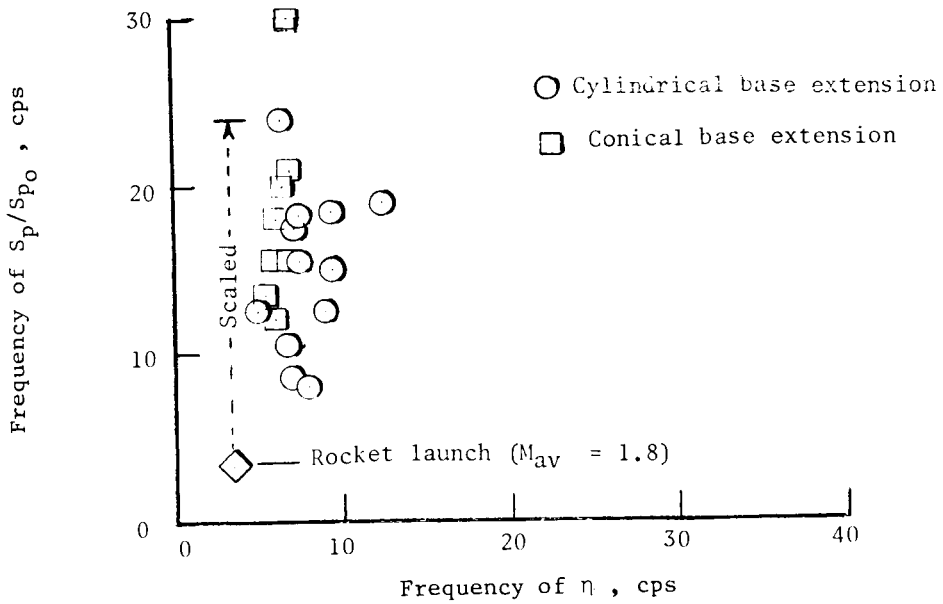

(a) M = 2.0.

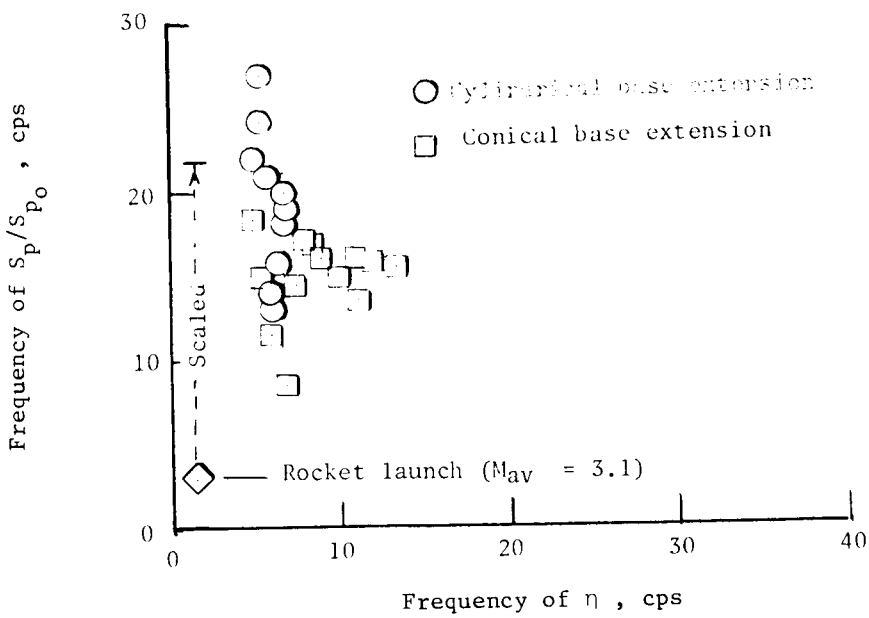

(b) M = 3.0.

Figure 13.- Effect of oscillation frequencies on canopy projected-area ratios with geometric porosity of 12.5 percent.

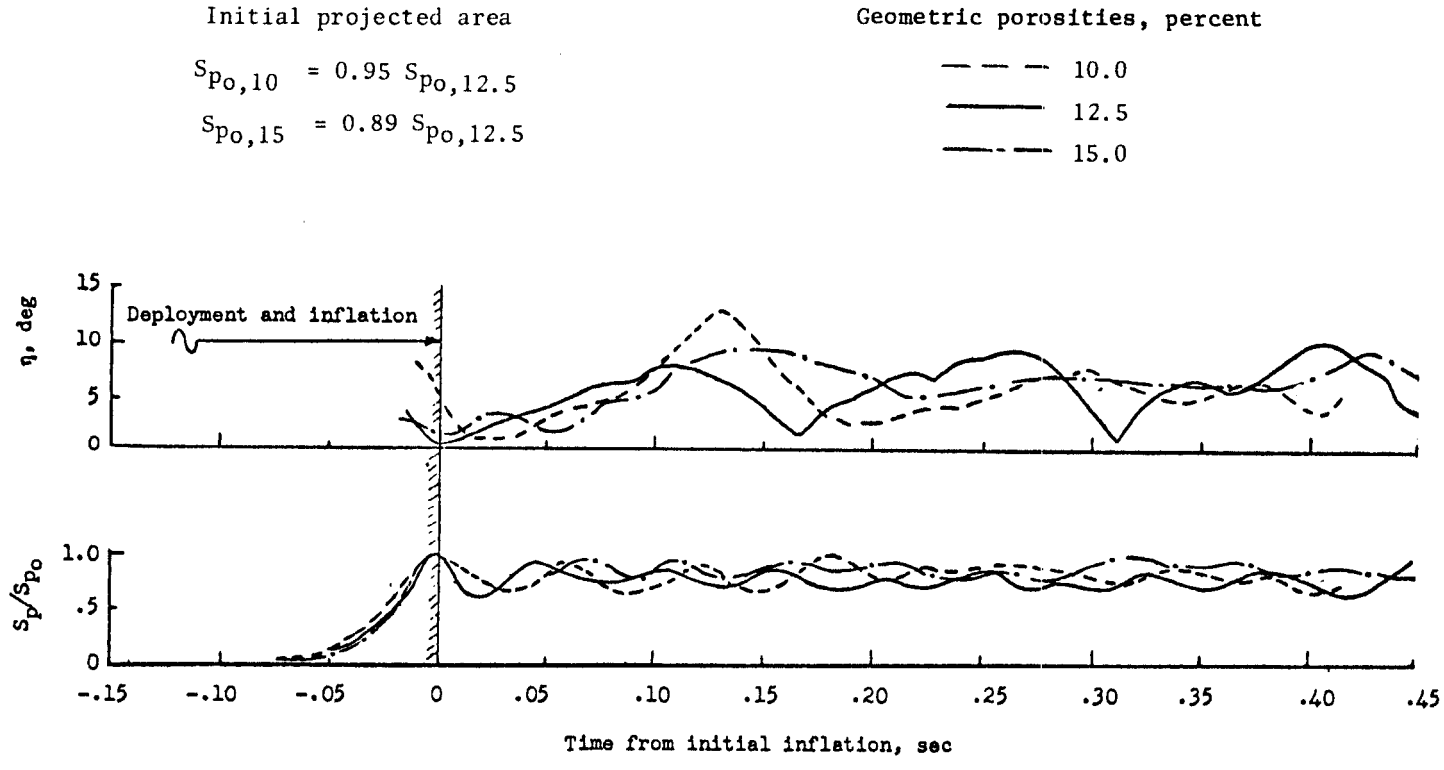

Figure 14.- Effect of geometric porosities on canopy motions and projected-area ratios at M = 2.0 with cylindrical base extension.

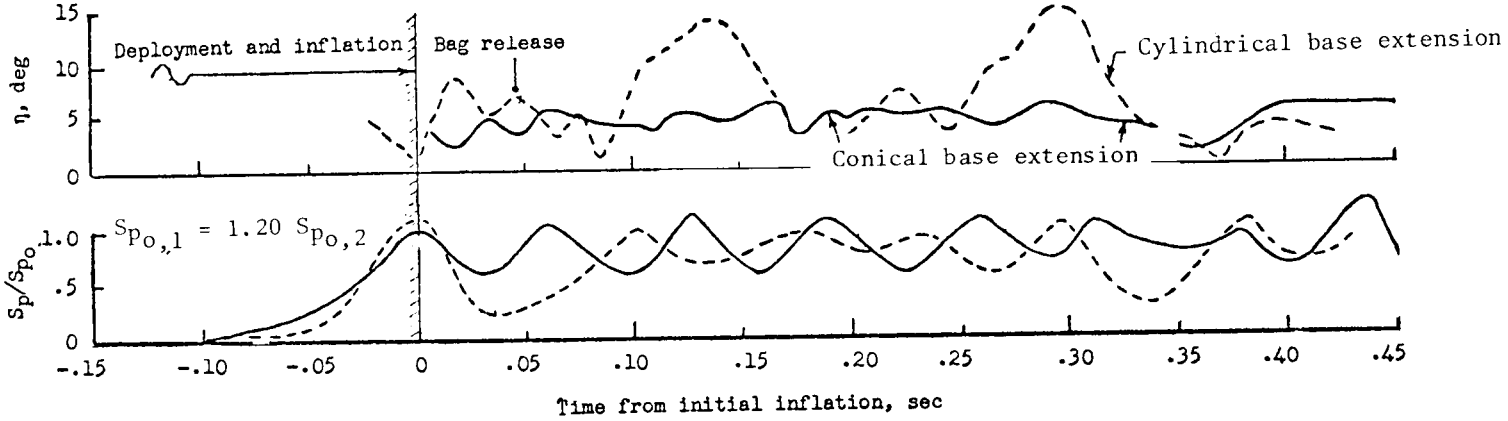

(a) M = 3.0.

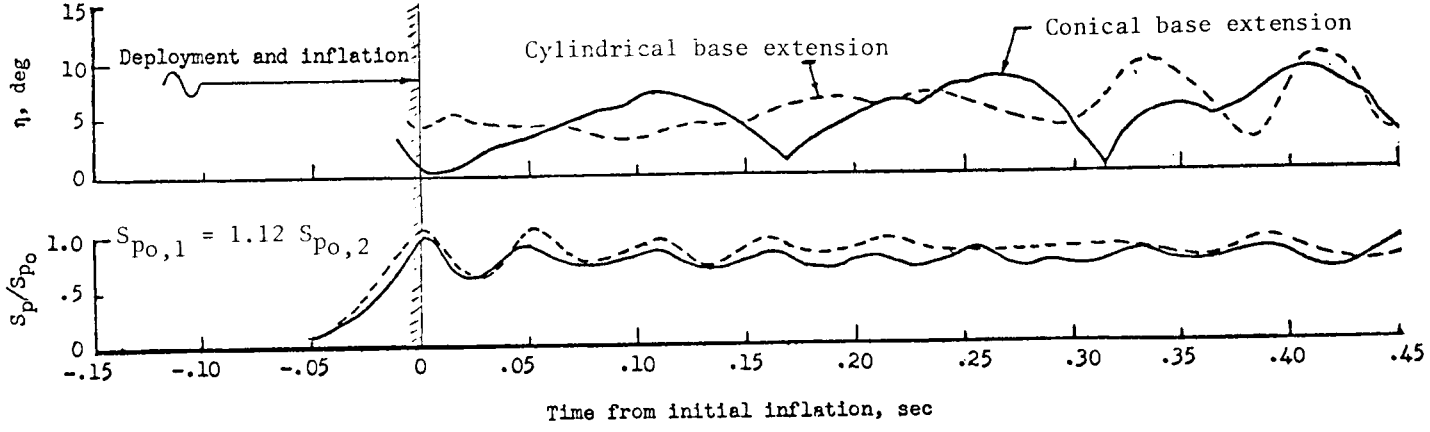

(b) M = 2.0.

Figure 15.- Effect of base-extension geometry on canopy motions and projected-area ratios (λ_g = 12.5 percent).

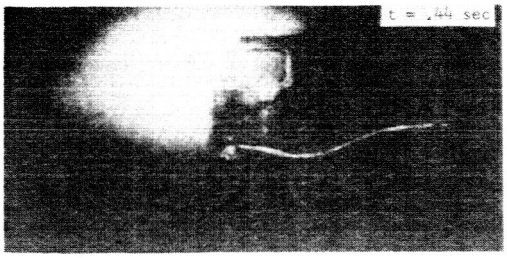

(a) Deployment.

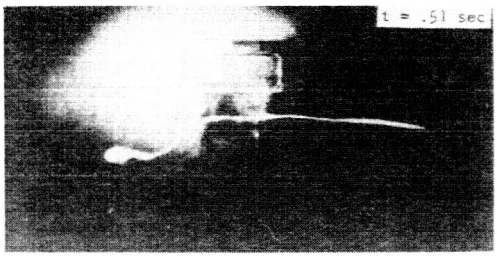

(b) Line strip.

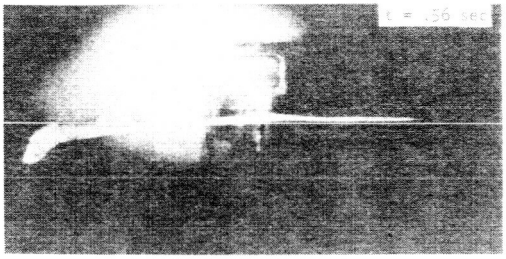

(c) Line stretch.

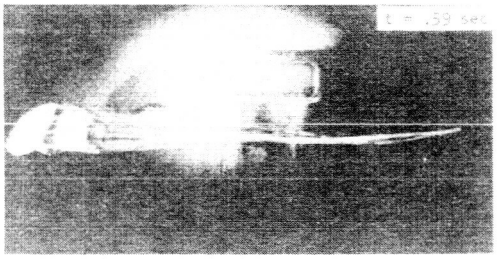

(d) Bag strip.

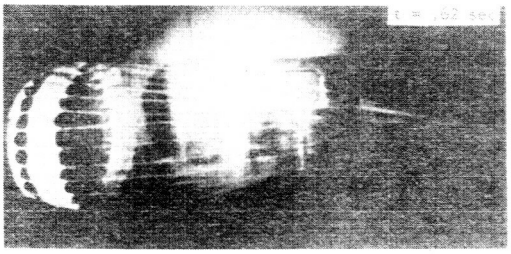

(e) Inflation.

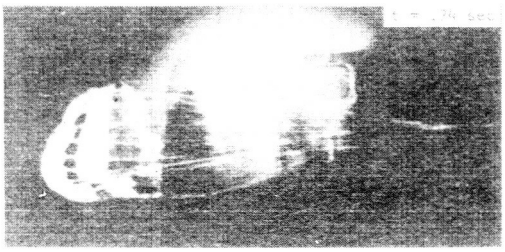

(f) Collapse.

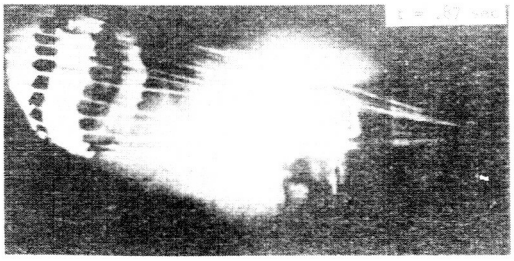

(g) Positive angle of attack.

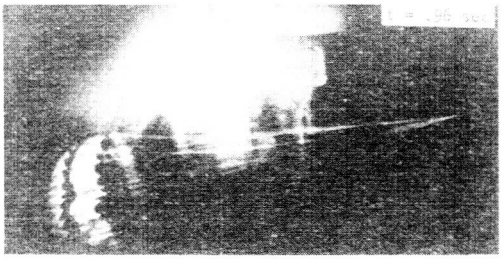

L-72-6500

(h) Negative angle of attack.

Figure 16.- Sequence photographs of deployment and inflation with suspension lines lengthened to $X/D_2 = 9.6$ behind the conical base extension at $M = 2.5$ $(\lambda_g = 12.5$ percent$)$.

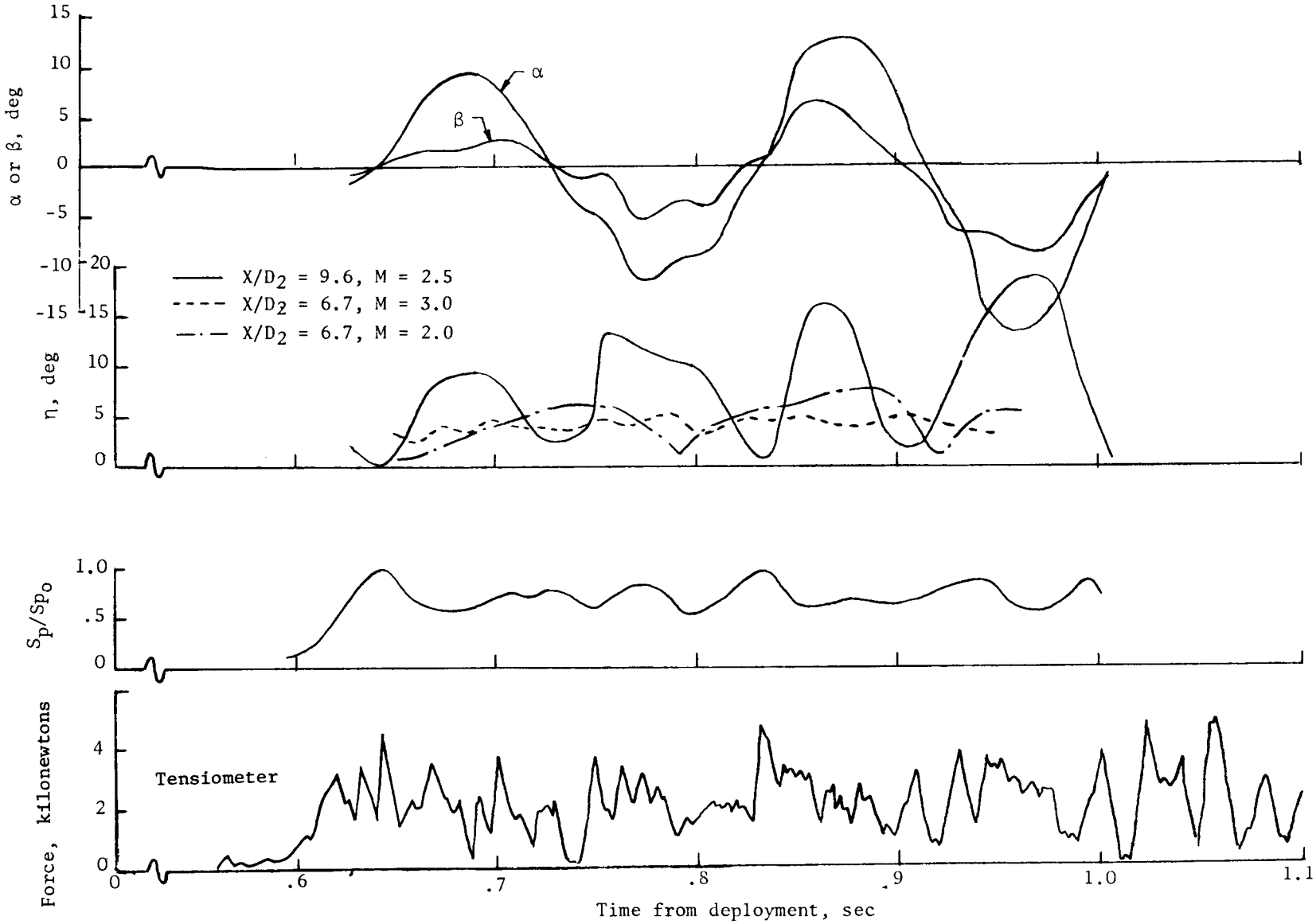

Figure 17.- Dynamic characteristics at M = 2.5 with suspension lines lengthened to $X/D_2 = 9.6$ behind the conical base extension $(\lambda_g = 12.5$ percent$)$.

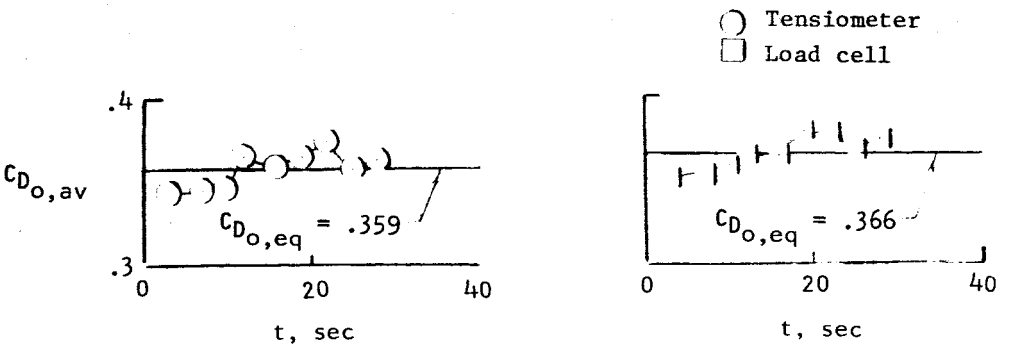

(a) λ_g = 10 percent.

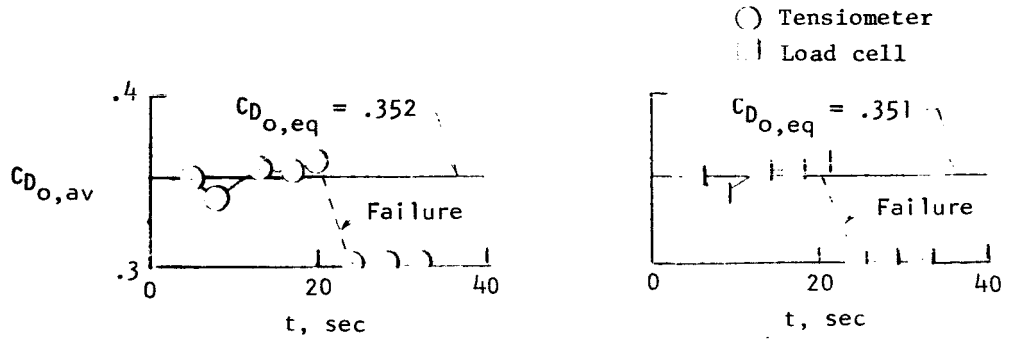

(b) λ_g = 15 percent.

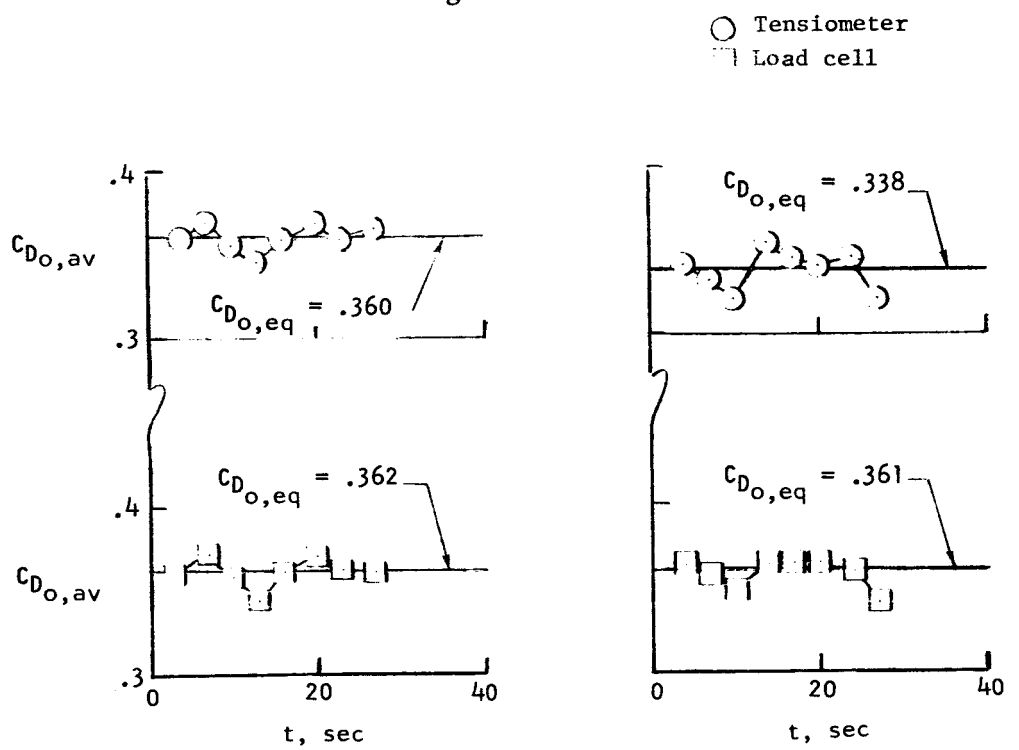

(c) λ_g = 12.5 percent.

Figure 18.- Equivalent drag coefficients for three geometric porosities at M = 2.0 with cylindrical base extension.

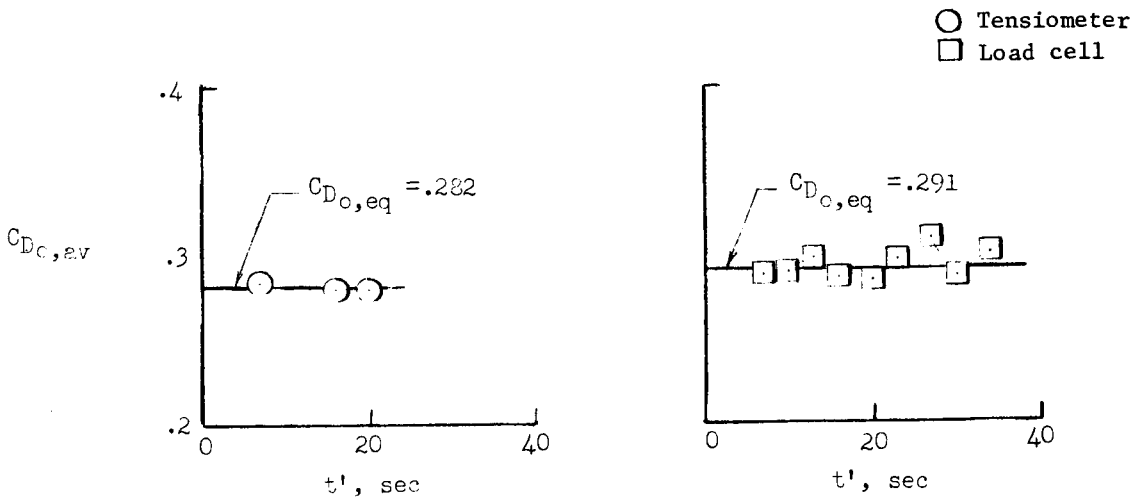

(a) λ_g = 10 percent.

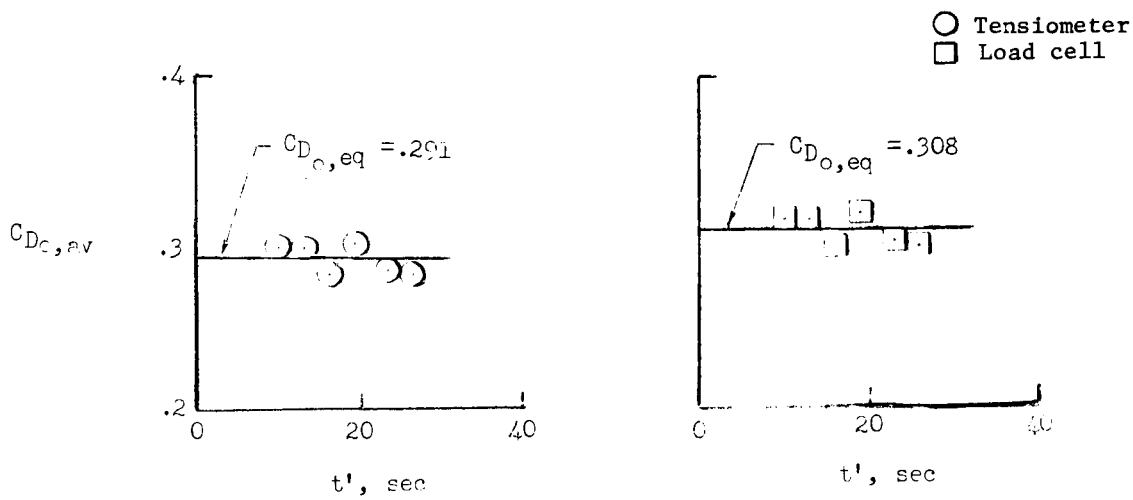

(b) λ_g = 15 percent.

Figure 19.- Equivalent drag coefficients for two geometric porosities at M = 2.5 with cylindrical base extension.

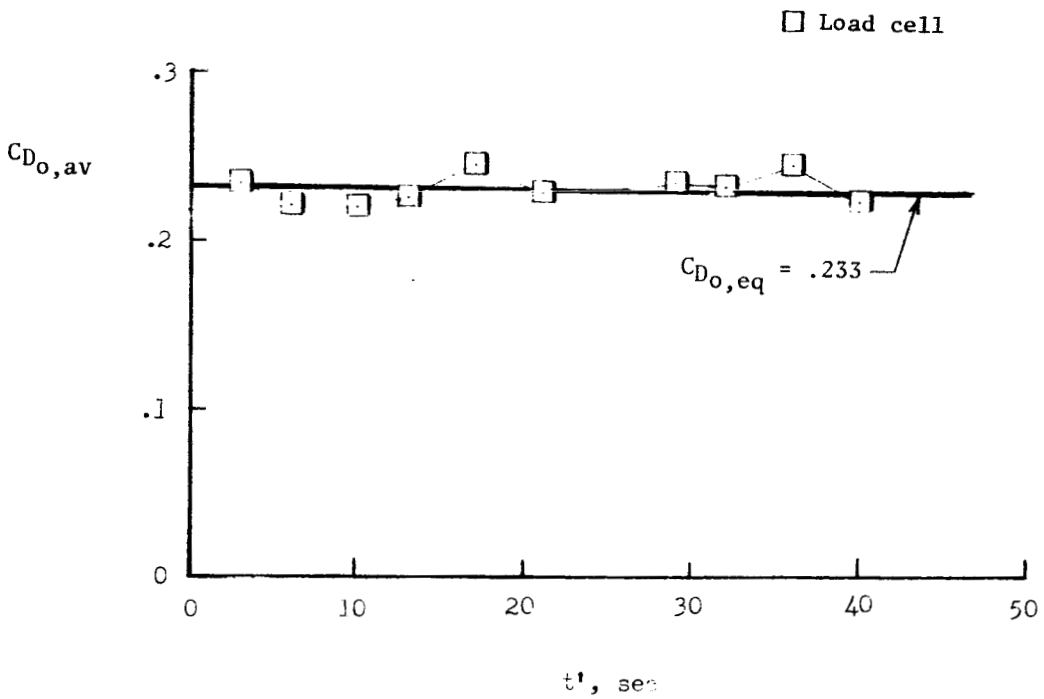

Figure 20.- Equivalent drag coefficients at M = 3.0 with cylindrical base extension (λ_g = 12.5 percent).

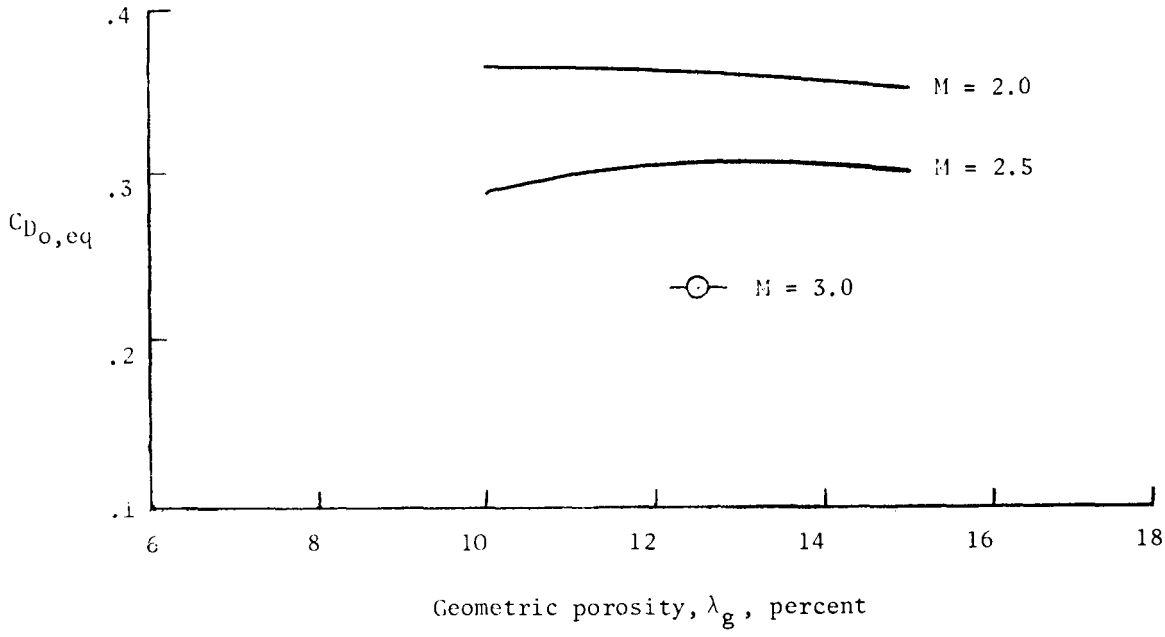

Figure 21.- Variation of equivalent drag coefficient with geometric porosity (cylindrical base extension).

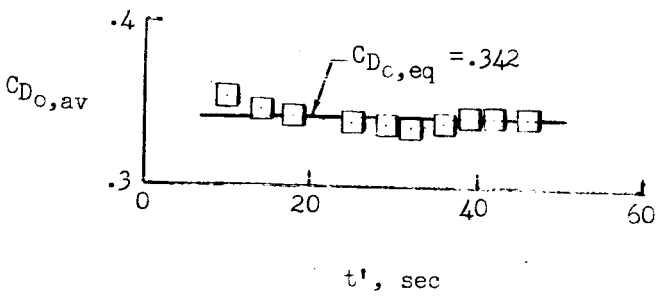

(a) M = 2.0.

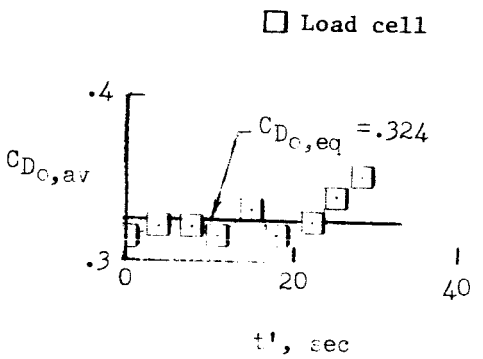

(b) M = 2.25 (locked base extension).

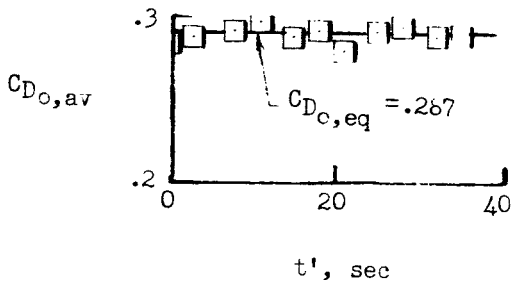

(c) M = 2.5 (locked base extension).

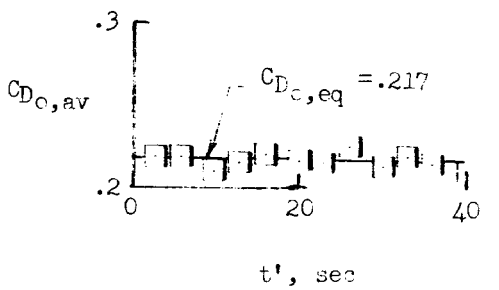

(d) M = 3.0.

Figure 22.- Equivalent drag coefficients for 12.5-percent geometric porosity and the conical base extension.

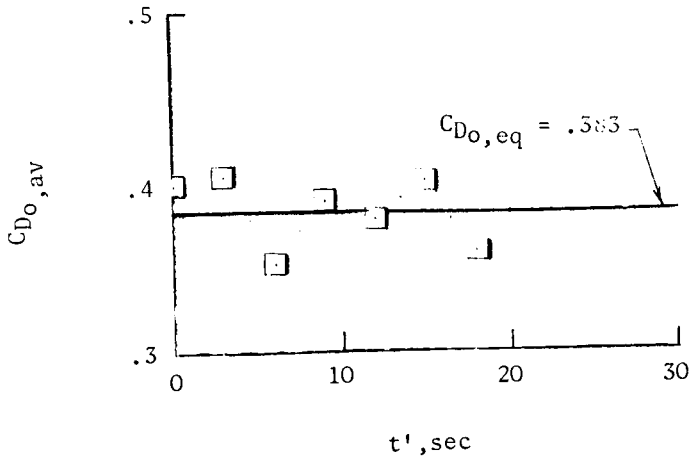

(a) Tensiometer.

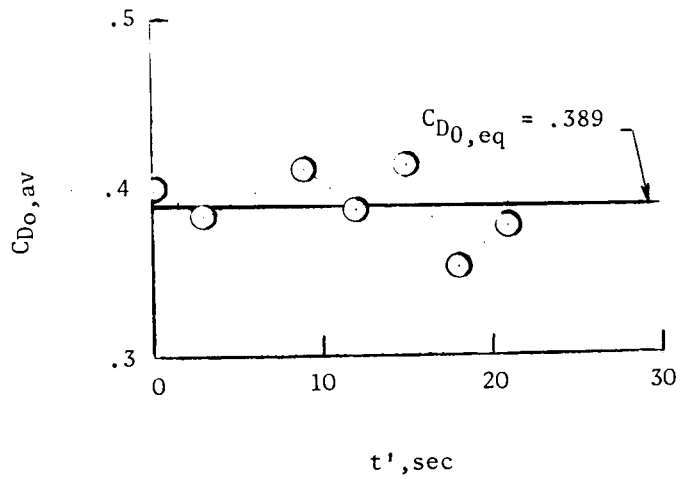

(b) Load cell.

Figure 23.- Equivalent drag coefficients at $M = 2.5$ for suspension lines lengthened to $X/D_2 = 9.6$ behind the conical base extension $(\lambda_g = 12.5$ percent$)$.

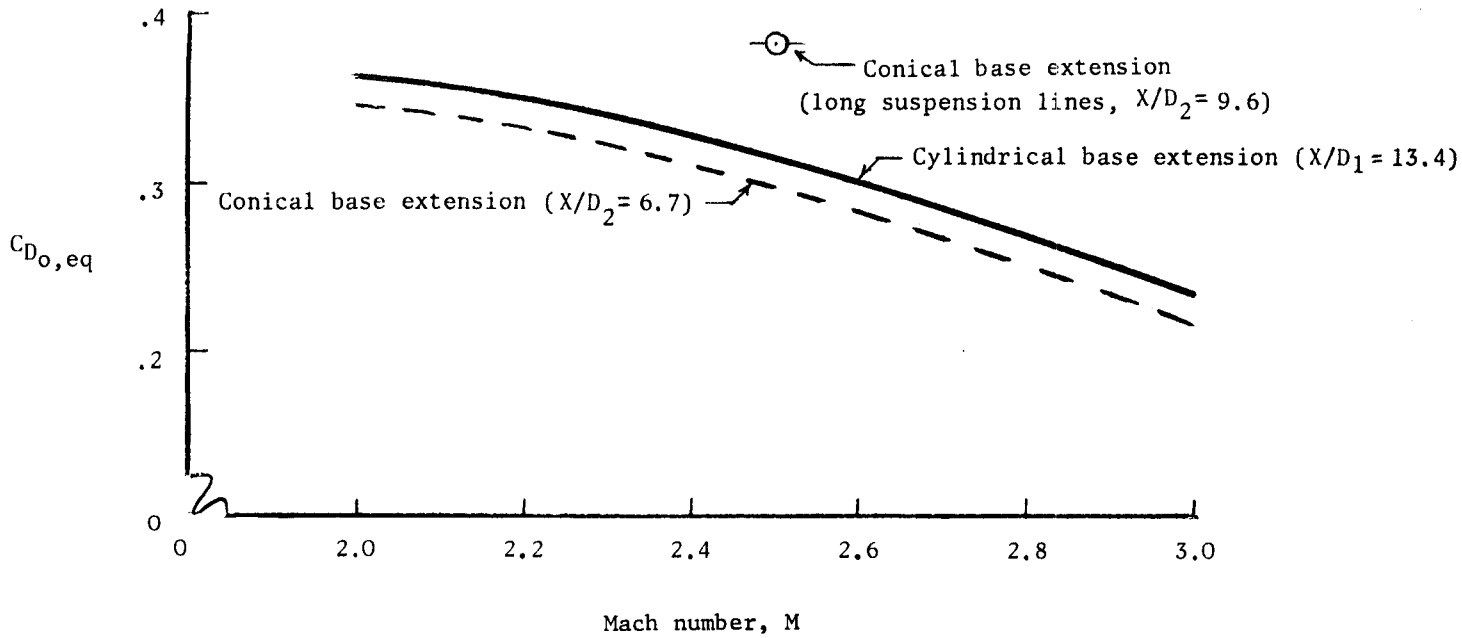

Figure 24.- Variation of equivalent drag coefficient with Mach number for the cylindrical and conical base extensions and increased suspension-line length (λ_g = 12.5 percent).

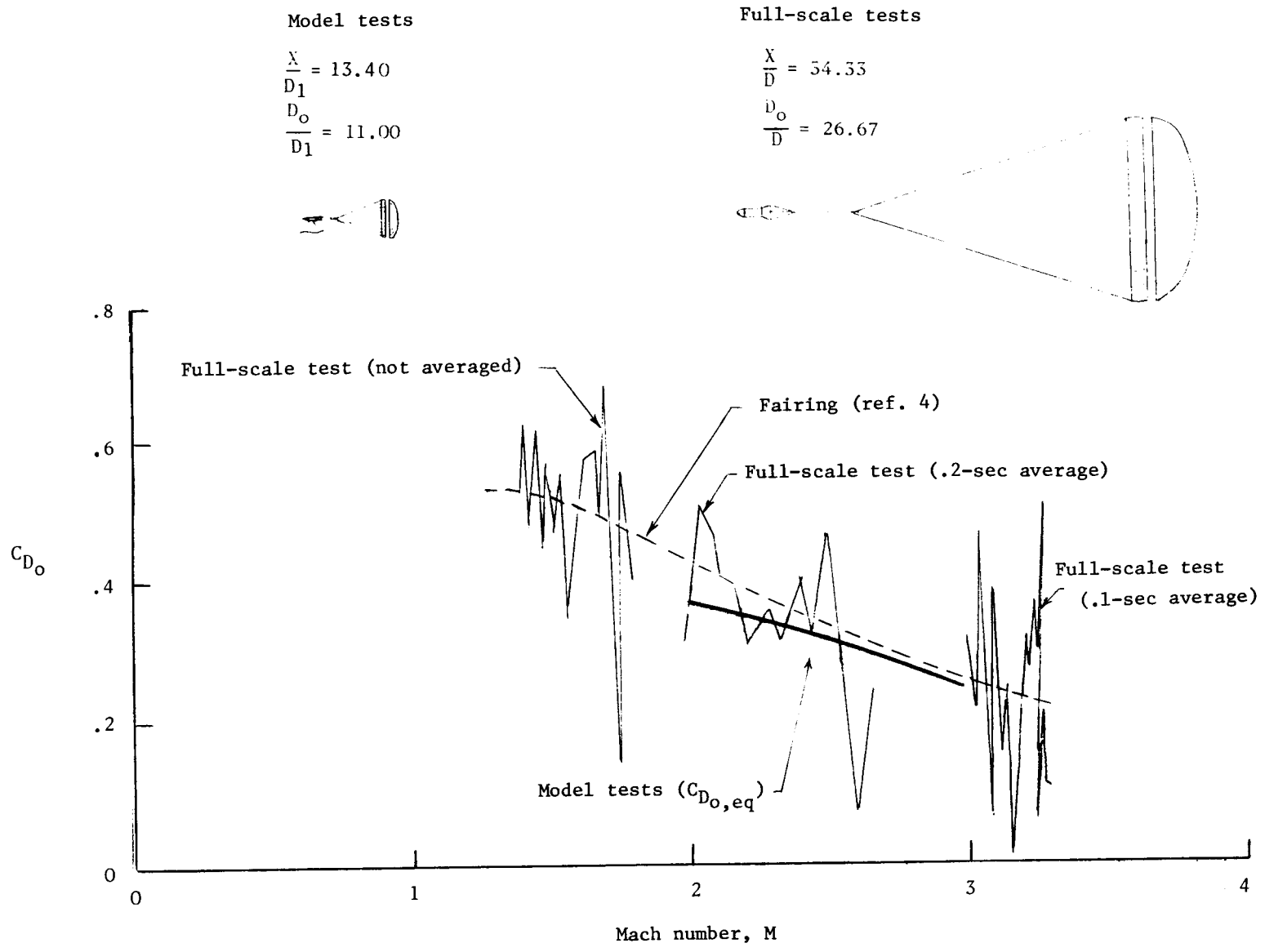

Figure 25.- Comparison of drag coefficients from model tests with full-scale flight results (λ_g = 12.5 percent).

NATIONAL AERONAUTICS AND SPACE ADMINISTRATION
WASHINGTON, D.C. 20546

OFFICIAL BUSINESS
PENALTY FOR PRIVATE USE $300

SPECIAL FOURTH-CLASS RATE
BOOK

POSTAGE AND FEES PAID
NATIONAL AERONAUTICS AND
SPACE ADMINISTRATION
451

U.S.MAIL

POSTMASTER: If Undeliverable (Section 158 Postal Manual) Do Not Return

"The aeronautical and space activities of the United States shall be conducted so as to contribute . . . to the expansion of human knowledge of phenomena in the atmosphere and space. The Administration shall provide for the widest practicable and appropriate dissemination of information concerning its activities and the results thereof."

—NATIONAL AERONAUTICS AND SPACE ACT OF 1958

NASA SCIENTIFIC AND TECHNICAL PUBLICATIONS

TECHNICAL REPORTS: Scientific and technical information considered important, complete, and a lasting contribution to existing knowledge.

TECHNICAL NOTES: Information less broad in scope but nevertheless of importance as a contribution to existing knowledge.

TECHNICAL MEMORANDUMS: Information receiving limited distribution because of preliminary data, security classification, or other reasons. Also includes conference proceedings with either limited or unlimited distribution.

CONTRACTOR REPORTS: Scientific and technical information generated under a NASA contract or grant and considered an important contribution to existing knowledge.

TECHNICAL TRANSLATIONS: Information published in a foreign language considered to merit NASA distribution in English.

SPECIAL PUBLICATIONS: Information derived from or of value to NASA activities. Publications include final reports of major projects, monographs, data compilations, handbooks, sourcebooks, and special bibliographies.

TECHNOLOGY UTILIZATION PUBLICATIONS: Information on technology used by NASA that may be of particular interest in commercial and other non-aerospace applications. Publications include Tech Briefs, Technology Utilization Reports and Technology Surveys.

Details on the availability of these publications may be obtained from:

SCIENTIFIC AND TECHNICAL INFORMATION OFFICE

NATIONAL AERONAUTICS AND SPACE ADMINISTRATION

Washington, D.C. 20546